Reliability Improvement of 1 Mil Aluminum Wire Bonds for Semiconductors

Technical Performance Summary

Final Report

Contract No. NAS8-26636
Contract Dates 6 Nov. 1970 - 6 Dec. 1971
Contract Amount $30,000.00

Prepared for
George C. Marshall Space Flight Center
National Aeronautics and Space Administration
Alabama 35812

Prepared by
MOTOROLA INC.
Semiconductor Products Divisi

K. V. Ravi - Project Leader (602) 273-6841

Ray White - Program Manager (602) 949-3482

Reliability Improvement of 1 Mil Aluminum Wire Bonds for Semiconductors

Technical Performance
Summary

Final Report

Contract No. NAS8-26636
Contract Dates 6 Nov. 1970 - 6 Dec. 1971
Contract Amount $30,000.00

Prepared for
George C. Marshall Space Flight Center
National Aeronautics and Space Administration
Alabama 35812

Prepared by
MOTOROLA INC.
Semiconductor Products Division

K. V. Ravi - Project Leader (602) 273-6841
Ray White - Program Manager (602) 949-3482

TABLE OF CONTENTS

LIST OF ILLUSTRATIONS

LIST OF ILLUSTRATIONS (Cont'd.)

SECTION I

1.0 INTRODUCTION

The reliability of semiconductor devices is strongly influenced by the reliability of wire bonds used in the assembly of the devices. Wire bond reliability can be roughly divided into two areas: (a) reliability or integrity of the bond during manufacture and testing, and (b) reliability during device operation. Reliability during manufacture affects the yield of packaged transistors. Such a problem is generally manifested in, for example, the inability to form a bond between the wire and metallization on the die, severe deformation of the wire, tearing or breaking of wire during bonding, etc. Most of these problems can be quickly identified with factors such as cleanliness, equipment malfunction, operator error, the choice of wrong materials, etc, and effective corrective measures can be taken.

Bond reliability during operation, on the other hand, is a more subtle phenomenon. A complete understanding of the nature of the failure mechanism involved is a first step in obtaining solutions to this catagory of reliability problems. Every aspect of the bonding operation influences bond reliability during service.

This report is concerned with one specific type of reliability problem that can occur during service. The failure mode associated with this form of reliability problem involves fracture of wire bonds as a result of repeated flexure of the wire at the heel of the bond when the devices are operated in an on-off mode. The mechanism of failure is one of fatigue induced fracture of the wire.

The driving force for flexure of the wire results from the differential thermal expansion of the material of the wire (aluminum) and the material of the package (Kovar) in which the

device chip is encased. The heat source is the semiconductor chip which generates heat at the p-n junction. Since this failure mode is prevalant only when the on-off cycle times are long (generally >1 minute) I^2R type heating of the wire does not play a large part in introducing flexure. However if the on-off times are faster than the thermal time constant of the package, then the ΔT, i.e. the temperature difference between the on and off stages is not high enough to appreciably flex the wire. Consequently this failure mode assumes significance when the on-off times are such that the package (and the wire) have sufficient time to equilibrate at the high temperature of operation and can cool to a low temperature approaching the ambient temperature during the off cycle. Figure 1a illustrates schematically the mechanism involved in the failure of the wire bond due to fatigue. Figure 1b shows scanning electron micrographs of a wire bond which failed as a result of fatigue.

Fatigue is the failure by fracture of a piece of metal which is subjected to cyclic stress. Failure of a member under a cyclic stress can occur at a stress level much below the minimum static (as opposed to cyclic) stress needed to produce deformation and fracture in the material. This means that the small degree of strain (which is proportional to stress) experienced by the wire bond during the on-off operating mode is sufficient to eventually result in the fracture of the wire after a certain number of cycles.

The general problem of fatigue induced failure can be approached from two points of view. One approach is to study the mechanics of the system, i.e. the magnitude, distribution and types of stresses and strains in the system and attempt to optimize these for maximum fatigue life through proper design and control during manufacture. A second approach is to evaluate the system from a materials science or metallurgical point of view since the phenomenon of fatigue is a very sensitive function of metallurgical variables

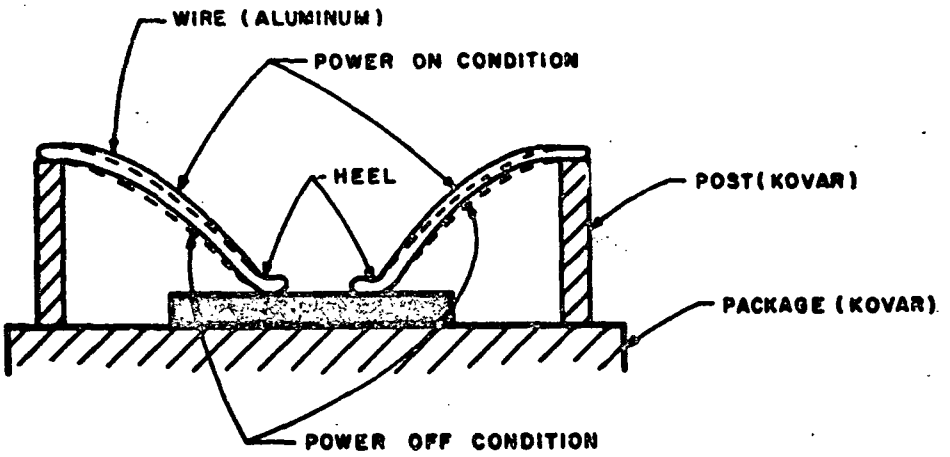

Failure occurs at the heel of the bond.

Figure 1 (a)

Stereo pair of scanning electron micrographs of a Al-1% Si wire bond which failed during power cycling. The crack has propagated through the heel of the bond.

Figure 1 (b)

9800-11-1

such as the strength and ductility of the metal, the microstructure, the impurity or alloy content and distribution, the surface quality, etc, of the member undergoing fatigue.

Obviously, the two areas associated with bond integrity, i.e. the design and the materials system used are not independent of each other. An overall improvement of the realiability requires that both these factors be considered. The aim of this research project has been to improve the reliability of a chosen transistor with respect to the failure mode discussed above. The design and manufacture of wire bond systems has evolved to a point where large numbers of reliable bonds are made in a manufacturing situation. Although certain improvements and controls can be incorporated into the existing manufacturing processes it is felt that major improvements in the overall reliability can be achieved primarily through a better understanding of the materials aspect of the bonding operation. This contention will be substantiated in subsequent sections of this report. The approach to the problem and the scope of the work is briefly presented below.

The primary variable examined has been the alloy composition and mechanical properties of the material of the wire bond. One-mil diameter wires of aluminum with various alloy additions have been studied. The method of testing these wires for fatigue characteristics is a main contribution of this work and consists of the design, construction and operation of an accelerated fatigue testing machine which permits rapid fatigue testing of wire bonds. Extensive use of the scanning electron microscope to correlate the fatigue data obtained on the accelerated fatigue testing apparatus with operational life times is another aspect of this investigation. The metallurgy of the wires with respect to microstructure, the kinetics of the growth of insoluble phases, etc, were studied using the electron microprobe. Other bonding variables such as the properties of the metallization on the die, the wire dressing,

variables associated with the bonding tool were examined briefly. However, as mentioned before, the primary emphasis has been on the materials aspect of bonding.

The vehicle employed for this study was the 2N2222 NPN transistor mounted in a gold plated TO-18 package and bonded with 1-mil diameter wires. Both thermocompression and ultrasonic bonding techniques were investigated.

Based on this study, recommendations for obtaining high reliability devices capable of withstanding 50,000 on-off cycles (1 minute on, 1 minute off) are made. Devices built according to these recommendations are being tested in the operating mode.

SECTION II

2.0 EXPERIMENTAL PROCEDURE

2.1 Accelerated Fatigue Testing

In view of the fact that the failure mode being investigated is a function of the number of on-off cycles experienced by the device, the time element in testing the devices becomes a major factor. On the basis of a 1-minute-on, 1-minute-off test, a time period of >1600 hours is required to complete 50,000 cycles. This becomes impractical in an investigation wherein a number of variables have to be considered to optimise the bonds for maximum fatigue life. As a result a major portion of this research effort was expended in developing and building an accelerated fatigue testing apparatus.

Figure 2 shows photographs of the equipment. The instrument consists of a cantilevered beam which can be moved in the vertical direction in a cyclic mode with the aid of an electric motor and an eccentric mounting. To the cantilevered beam are attached a series of sliding fixtures which have sets of four vertical needles fixed in them. These sliding fixtures and the pins can be moved along the length of the cantilevered bar to obtain different amplitudes of vertical movement. The bar nearest the motor experiences the maximum movement.

Beneath the cantilevered bar are mounted a set of sliding device holders which contain sockets for TO-18 packages. These holders can also be moved in machined slots along a base plate parallel to the cantilevered bar. The fixtures containing the needles and the devices are positioned such that the wire bonds are directly beneath the needles and fixed in place. The needles can

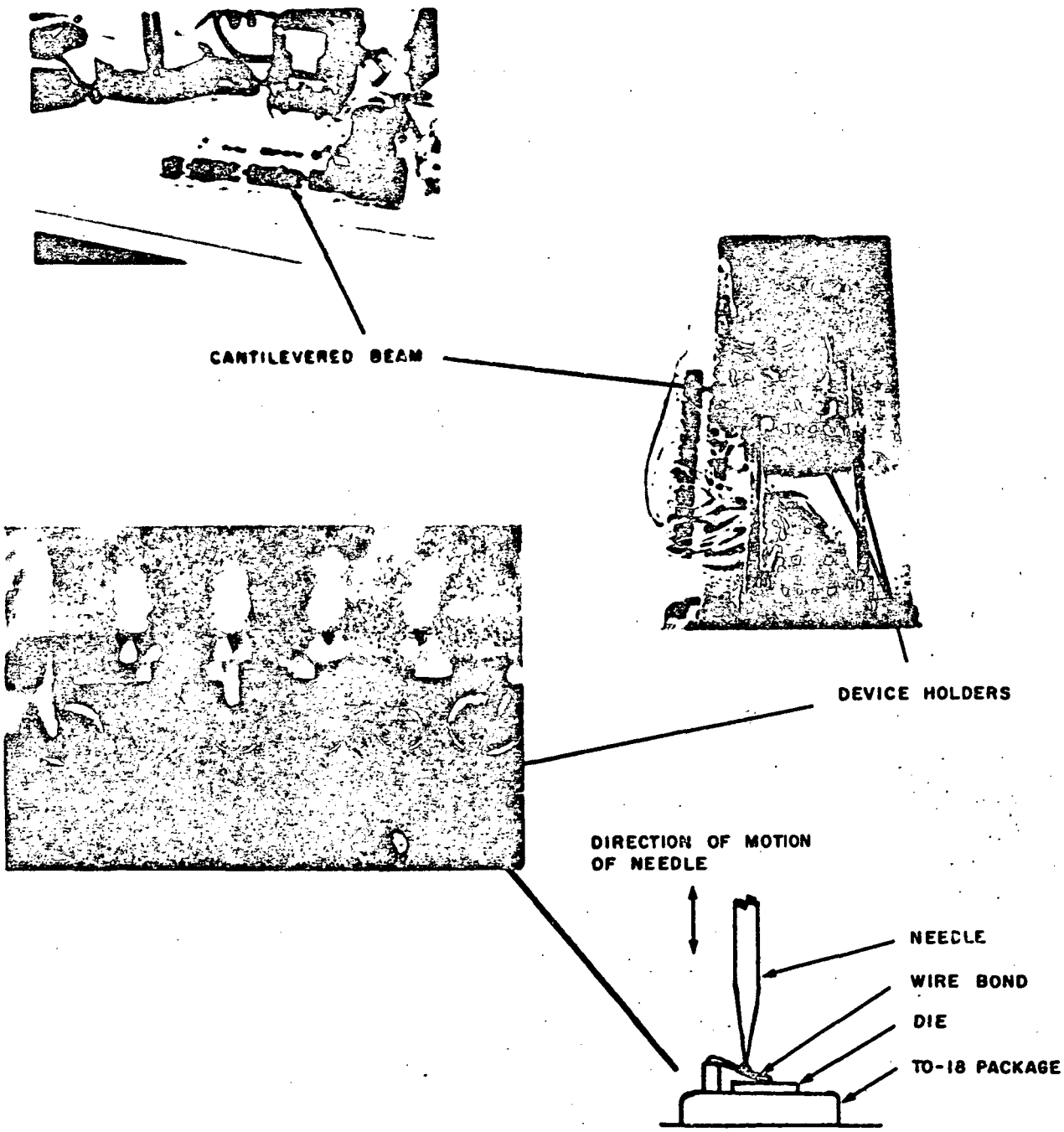

Figure 2. The accelerated Fatigue Testing Apparatus

be moved so as to be almost in contact with the wire bond at a position away from the heel of the bond. The needles are then cemented to the wire bonds by means of a conducting cement.

The vertical movement of the needle is conveyed to the wire bond simulating the flexure at the heel that occurs during power cycling. Since the frequency of flexing is ~30 cycles per second in this machine, it is possible to reach 50,000 cycles in less than one hour. The devices are connected to a chart recorder and a power source is used to detect the time at which failure occurs through fracture of the wire bond.

The entire apparatus is rigidly mounted to a firm support to eliminate extraneous vibration. Data was accumulated by obtaining the number of cycles to failure for different bonds. Since fatigue is statistical in nature it is necessary to test a number of specimens for each data point. Consequently, at each deflection of the wire, a number of tests were made and the data reported in subsequent sections represents average values of a number of readings.

The instrument was initially calibrated to determine the degree of motion of the cantilevered bar at different points along the bar by using sensitive dial gages. The speed of rotation of the electric motor and hence the number of deflection per unit time was obtained by using a strobe lamp of known frequency.

2.2 MECHANICAL PROPERTIES AND STRUCTURAL ANALYSIS

The mechanical properties (yield strength, tensile strength and ductility) of the wires were measured on a floor model Instron. Gage lengths of 1 inch were used at a strain rate 0.05 inch/minute. Using the small gage lengths resulted in a more representative test which could differentiate between wires with greater sensitivity.

The effects of heat treatments that a bonding wire experiences during operations such as bonding (thermocompression), stabilization bakes, etc, were studied by aging the wire at different temperatures in an inert atmostphere and mechanically testing on the Instron. Tests were always repeated a number of times to assure reproducibility.

Structural analysis of the wires was conducted in an electron probe microanalyzer. Since a primary effect of high temperature annealing on fatigue characteristics is in changing the type and distribution of impurities of second phases (such as silicon in aluminum) the microprobe is ideal for obtaining this type of information. For microprobe analysis wires subjected to different heat treatments were encapsulated in plastic, polished flat, and examined in the instrument.

The scanning electron microscope was used extensively throughout this investigation for close examination of bond quality, the mode of failure, etc. The SEM was also used to obtain data on the degree of deflection experienced by the wire when operated in a 1-minute-on, 1-minute-off mode. Since the flexure of the wire is a consequence of the thermal excursion of the package, the heat transfer characteristics of the package as well as the heat sink employed and the type of ambient atmostphere are important. In the SEM the sample is in a vacuum (10^{-4} to 10^{-5} Torr) and hence the heat dissipation from the package is less efficient than in air. Consequently, in a 1-minute-on, 1-minute-off test, the package becomes hotter during the on cycle when the device is in the vacuum chamber of the SEM as compared to its normal operating ambient in air. In order to overcome this problem, accurate measurement of the package temperature (with the lid off) was made with the device outside the SEM. The device was then mounted inside the SEM and

and turned on. The temperature was continuously monitored until the package reached the same temperature as it did after 1 minute in air. At this point the wire was photographed at the high magnification of the SEM and the device turned off. A second photograph of the wire was taken when the device had cooled to room temperature.

SECTION III

3.0 RESULTS AND DISCUSSION

3.1 FATIGUE AS A FAILURE MODE

Although it has been known for some time that flexure of the wire can lead eventually to failure, no in-situ observation of the failure mode associated with the long on-long off (as opposed to fast pulsed mode) has been reported. In order to verify that repeated bending of the wire due to cyclic operation of the device leads to fracture at the heel of the bond an accelerated test was performed in the scanning electron microscope and the resulting flexure and failure of the wire observed in-situ. The SEM was operated with a rapid scan attachment and the dynamic information recorded on video tape.

The device was mounted in the SEM with a copper grid just behind the device to serve as a reference source to detect and measure the degree of motion (see Figure 3). To accelerate the failure of the bond, the device was operated beyond its rated capacity. The unit was electrically pulsed with 2.4-millisecond pulses applied to the collector-emitter terminal at a 30Hz rate. A base current of ≈ 1mA was constantly applied to allow an I_c of 100 mA during pulsing at 10V. This resulted in a power dissipation of 1 watt which is twice the rated capacity of the device.

Figure 4 shows a series of scanning electron micrographs obtained from the video tape at different times in the course of the experiment. The micrographs 4(1) and 4(2) show the heel of the wire before the start of the pulsing operation. Figures 4(3) and 4(4) were obtained after approximately 2 seconds of pulsing. The micrographs show that the wire is beginning to fracture at the heel (shown by the arrow). Although only a few on-off cycles have

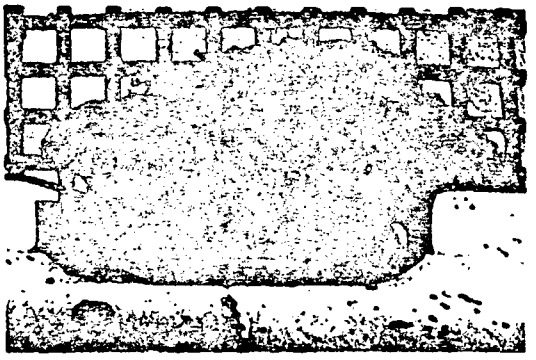

Figure 3. SEM Photograph of a 2N2222 Device showing the Wire Bonds. The sample has been tilted in such a way as to obtain a view of the wires when they move during power cycling. The grid in the background is used as a reference source.

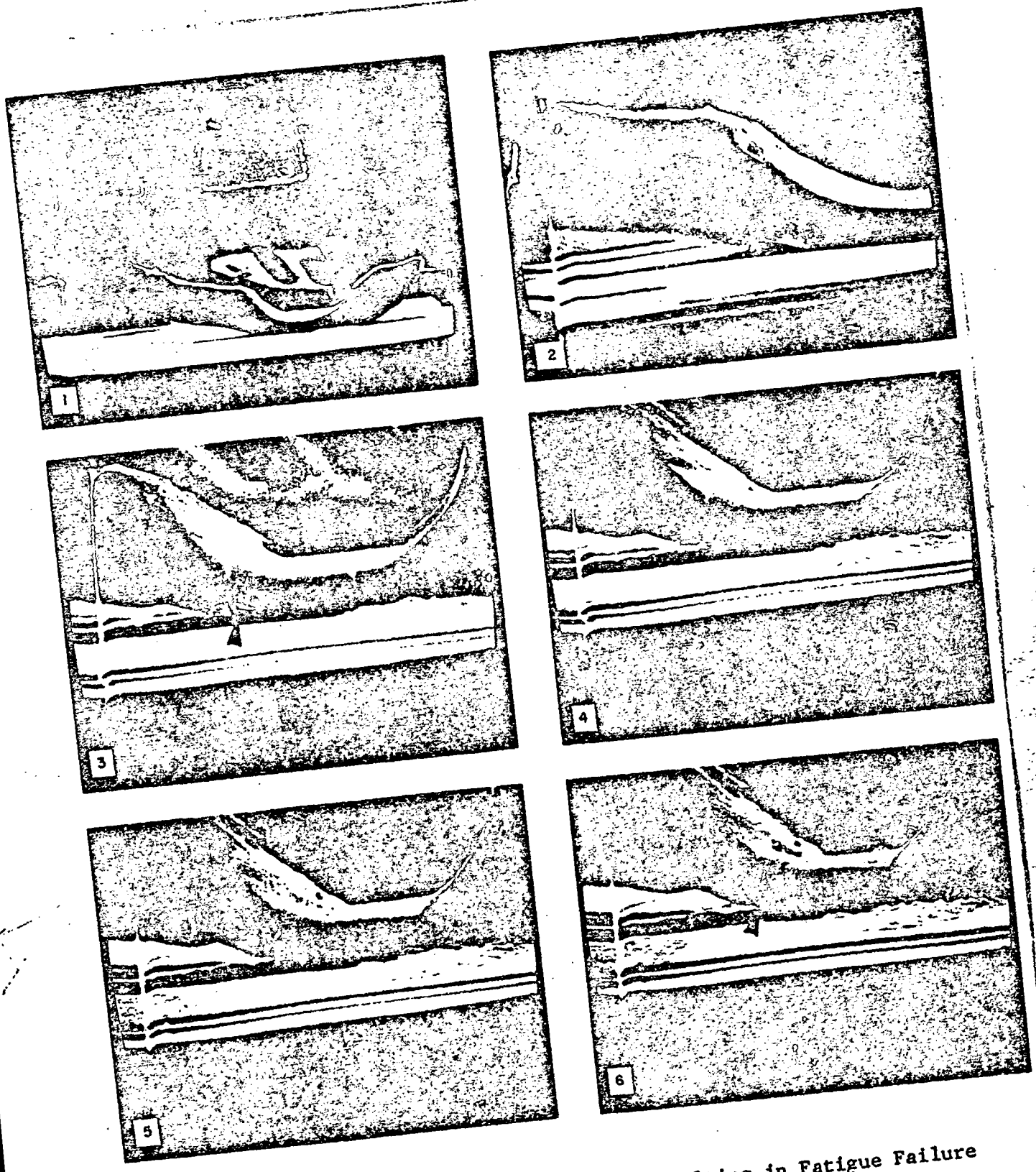

Figure 4. Rapid Pulsing of Wire Bond Resulting in Fatigue Failure

9803-11-1

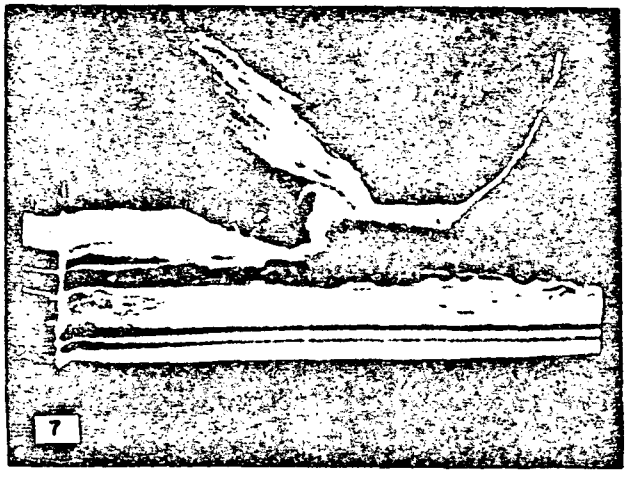

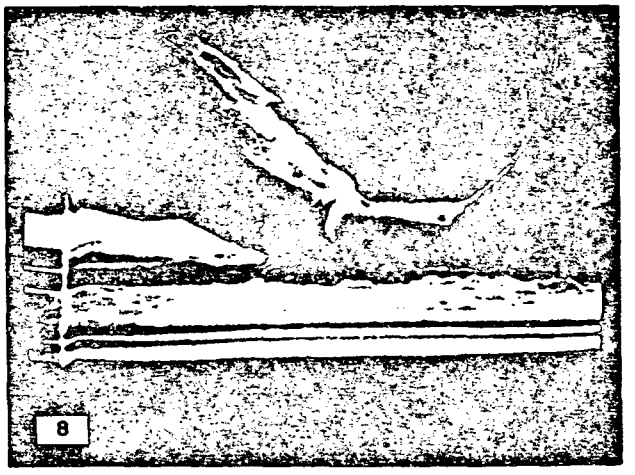

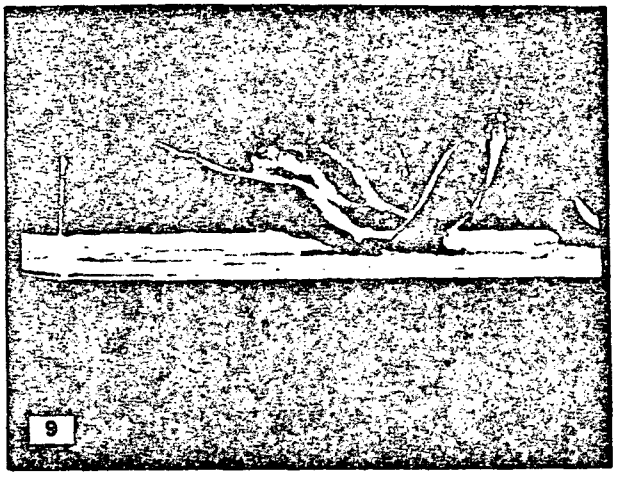

APPARENT MOTION OF SPECIMEN DURING PULSING DUE TO ELECTROSTATIC AND MAGNETIC DEFLECTION OF ELECTRON BEAM.

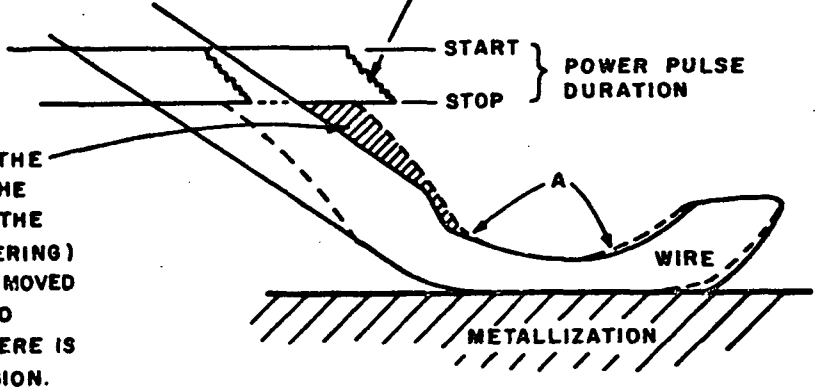

THIS DUAL IMAGE IS DUE TO THE OVERLAPPING OF IMAGES OF THE FIRST (UNPOWERED) SCAN AND THE FOLLOWING SCAN (AFTER POWERING) AT WHICH TIME THE WIRE HAS MOVED DUE TO HEATING. AT A THE TWO IMAGES ARE ALIGNED SINCE THERE IS NO MOTION AT THE BONDED REGION.

Figure 4 (Cont'd.)

elapsed the severe stressing of the wire due to large power being dissipated by the device results in the initiation of cracks. Figure 4(5) represents a micrograph obtained 50 seconds after the start of pulsing showing further progression of the cracks. Figures 4(6) and 4(7) show the severe damage taking place at the heel after approximately 60 second and 75 seconds from the start. The initiation of more cracks is evident in Figure 4(6)(shown by the arrows). Figures 4(8) and 4(9) show the final failure of the bond. A total time of approximately 90 seconds had elapsed before failure was observed. The important fact that failure due to fatigue occurs at the heel of the bond has been confirmed by this experiment.

The pulsing experiment was also used to measure the deflection of the wire (at the heel) when subjected to this accelerated test by making use of the fact that at sufficiently short pulse times the wire will move between scans of the electron beam and hence a double image of the wire representing the position of the wire before and during the electrical pulse will be recorded on the same photomicrograph. All the micrographs in Figure 4 show the presence of this double image. The sketch in Figure 4 shows in detail the features observable in the micrographs and the method by which the deflection of the wire can be accurately measured. Using this technique the motion at the heel of the bond was measured to be approximately 1.3 microns at the initial stages of pulsing (from Figure 4(4)). And approximately 2.1 microns at the final stages when failure was anticipated (from Figure 4(5)). As can be observed in Figures 4(7) and 4(8) the flexure apparently increases as failure approaches. This is explainable on the basis that once the initial cracks have developed in the wire it is weakened considerably, and for the same power level more of the motion of the wire is conveyed to the heel of the bond. Consequently, the catastrophic nature of fatigue results in the initial crack generation leading to greater motion of the wire at the heel and hence the generation of more cracks.

An added feature of the micrographs in Figure 4 is the observation of the severe reconstruction of the surface of the aluminum metallization on the die. With increasing numbers of pulses the surface of the aluminum becomes progressively rougher. This roughening is also evident in Figure 1. The possible mechanisms for surface roughening of the aluminum have been discussed elsewhere[1] and will not be further pursued in this report except to note that the observation of the rough surface is a strong indication of the fact that the device has experienced repeated on-off power cycles.

The experiment discussed above is not to be construed as being identical to that of a conventional life test where the devices are subjected to long on-off cycles (e.g., 1 minute on, 1 minute off). This test was delibrately performed to demonstrate the nature of fatigue and is a far more drastic case than is observed during normal operation. However the essential mechanism of failure is the same in either case. Since fatigue is a function of both the magnitude of the stress level applied and the duration of the cyclic stress, a structural member will fail if either one or both these factors are changed.

3.2 VARIABLES AFFECTING FATIGUE

When a metal is subjected to repetitive or fluctuating stress it will fail at a stress much lower than that required to cause fracture on a single application of load. The basic method of presenting engineering fatigue data is by means of the S-N curve, which represents the dependence of the life of the specimen, in number of cycles to failure N, on the maximum applied stress S. Figure 5 shows an idealized sketch of an S-N curve for an aluminum alloy. The number of cycles a metal can endure before failure increases with decreasing stress. Generally N is taken to be the

(1) Philofsky, E., K. V. Ravi, E. Hall, J. Black; Surface Reconstruction of Aluminum Metallization - A New potential wearout mechanism; 9th Annual Proceedings, Reliability Physics, P.120 (1971)

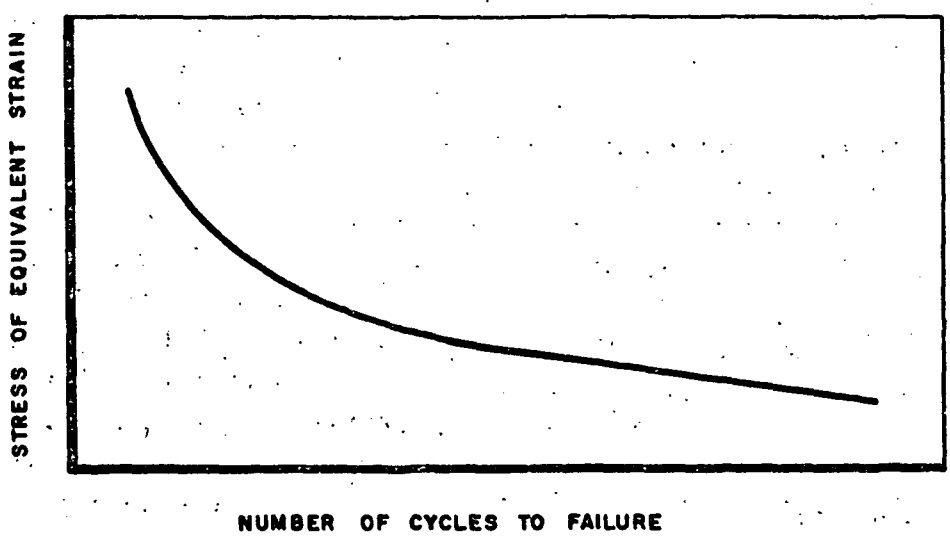

Figure 5. Idealized S-N Curve for a Typical Aluminum Alloy Which Does Not Exhibit a Fatigue Limit.

number of cycles of stress required to cause complete failure by fracture. This is made up of the number of cycles to initiate cracks and the number of cycles to propogate the cracks. For certain materials like steel and titanium, the S-N curve becomes horizontal at a certain limiting stress. Below this limiting stress called the fatigue limit or the endurance limit the material can presumably endure an infinite number of cycles without failure. Most nonferrous metals such as aluminum, copper, etc, do not exhibit a fatigue limit. The S-N curve continues to slope gradually downward with increasing number of cycles. This implies that failure by fracture will occur after a certain number of cycles, no matter how small the level of the applied stress.

However, in the relatively flat region of the curve shown in Figure 5 a small decrease in the stress (or equivalent strain) will result in a very large increase in the lifetime. For all practical purposes, and with special reference to wire bonds, the stress (or strain) experienced by the member is such that its value lies near the flat portion of the fatigue curve. Consequently, even though aluminum alloys do not exhibit a finite fatigue limit, if the entire fatigue curve is shifted slightly upwards through suitable alloying of the aluminum a very large increase in the lifetime can be obtained.

Fatigue life is a statistical quantity and hence considerable deviation from an average S-N curve determined with only a few specimens is to be expected. Each specimen has its own fatigue limit, a stress above which it will fail and below which it will not, and this critical stress varies from specimen to specimen for many reasons. Consequently, it is not possible to test one specimen and determine the fatigue life of all specimens based on the one data point. A suitable sample size should be selected to give an average value of the fatigue life at any specific stress level.

The major factors that influence the fatigue life of a metal are as follows:

(1) Design considerations
(2) Stress concentration effect
(3) Effect of metallurgical variables

(1) Design considerations such as the reduction in stress concentrations in the material and the use of beneficial compressive residual stresses can go a long way towards increasing the fatigue life of a metal. In the case of wire bonds design factors such as wire loop height, the degree of deformation at the heel of the bond, the surface quality of the wire at the heel, etc, play an important part in the overall reliability. Some of these factors will be discussed in greater detail in a subsequent section of this report.

(2) A significant factor in reducing the fatigue life of metals is the surface quality of the member undergoing fatigue. The fatigue strength is seriously reduced by the introduction of a stress raiser such as a notch, a crack or a hole. The presence of a notch results in three effects: (1) an increase in the concentration of stress at the root of the notch; (2) a stress gradient from the root of the notch toward the center of the specimen; and (3) a triaxial state of stress.

Figure6(a) is a plot of the stress (or the equivalent stress) needed to produce fatigue failure as a function of the number of on-off cycles to which the material is subjected. The higher the stress level, the fewer the cycles that are needed for the member to fail in fatigue. Two sets of curves are shown in Figure6(a), for a notched and an unnotched specimen. Introduction of a notch reduces the fatigue life significantly, i.e. for the

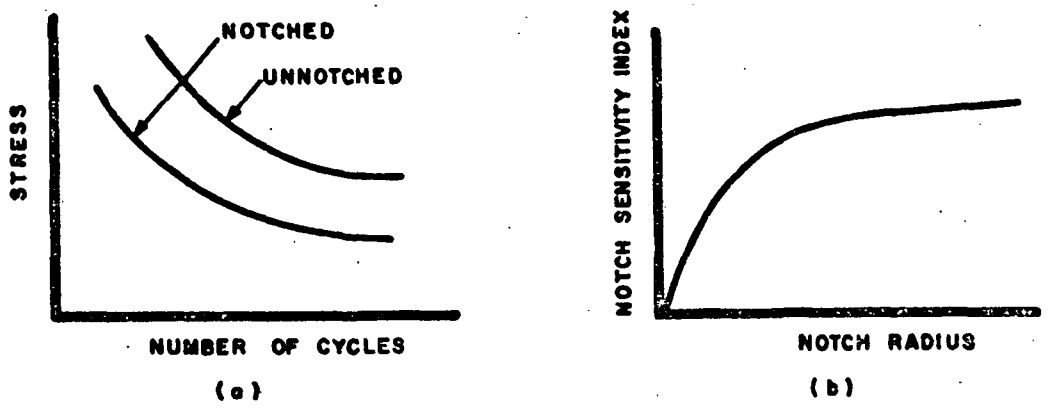

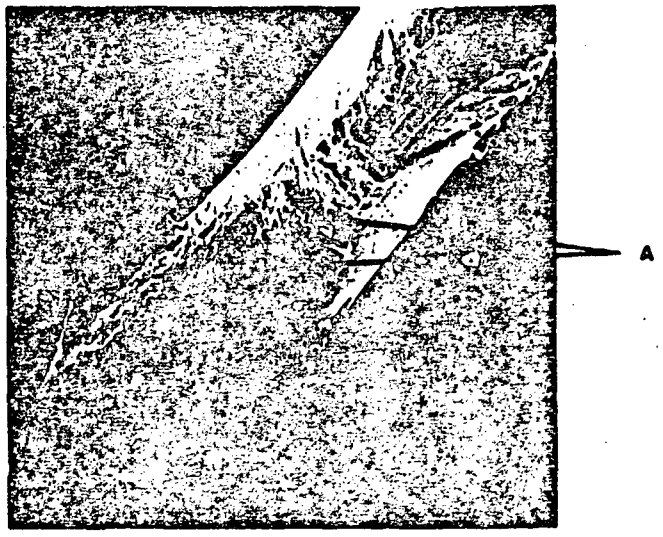

(c)

Figure 6. The effect of a Notch on Fatigue Properties

same stress level (or strain level corresponding to movement of the wire bond under a cyclic operation mode) the wire will fail after a much smaller number of cycles when a notch is present in the wire than in the absence of a notch.

The effect of a notch is more complex than just the reduction in wire cross-sectional area it produces. Figure 6(b) shows a plot of the notch sensitivity index as a function of the radius of the notch. The notch sensitivity index includes factors such as the theoretical fatigue limit of the material, the magnitude of stress concentration at the root of the notch, etc. It can simply be described as the propensity for failure of the material when a notch is introduced into the surface. As shown in Figure 6(b), the notch sensitivity increases with increasing radius of the notch and reaches an approximately constant value above a certain notch radius. This indicates that, everything else being equal, a sharp notch is less detrimental than a broad notch. However, in a practical case, the other factors can never be controlled to be equal. For example, it is impossible to tell (non-destructively) how deep a sharp notch goes. Hence, since the notches introduced into the heels of wire bonds can vary in type it is imperative that notches be avoided altogether to improve fatigue life. Figure 6 (c) shows an example of a wire bond with sharp notches (shown at A) introduced at the heel. These notches (cracks) were introduced by the bonding tool during bonding and the resulting bond is a problem case for potentially poor fatigue performance. A first step in improving lifetime of devices operated in an on-off sequency should be in the minimization of notch depth in wire bonds through better bonding techniques. (See Appendix I for further discussion on the effects of cracks and notches).

(3) Perhaps the most important of the variables that affect fatigue, and in particular the fatigue of wire bonds, are the metallurgical variables. The details of the mechanism of the initiation and growth of fatigue cracks are not yet fully resolved. However, considerable evidence exists to show that fatigue cracking is a phenomenon that is initiated by alternate slip of the material under the action of cyclic loading. During the initial stages of stress, slip bands are produced in favorably oriented grains. Each cycle of stress results in the generation and motion of new dislocations since slip or plastic deformation is achieved by the motion of dislocations. Some of these dislocations are thought to accumulate in certain favorable regions on slip planes near the surface of the sample, forming a nucleus of a growing fatigue crack. On the basis of this mechanism of fatigue, a correlation should exist between the fatigue characteristics of a metal and its plastic properties since dislocations play a more or less common role in both these processes of metal deformation. The one possible distinction between fatigue and plastic flow lies in the requirement that a specific kind of coalescence of accumulated dislocations is needed to form a fatigue crack whereas no such coalescence of dislocations is required to plastically deform the metal.

In view of the above discussed mechanism of the common role played by dislocations in fatigue and plastic properties (such as yield strength, tensile strength, and ductility) of metals, the metallurgical variables that affect one will affect the other.

The common metallurgical variables of relevance to the fatigue problem are briefly discussed below.

(a) The alloy content of the metal: Addition of alloying elements to pure metals is known to improve the mechanical

properties in terms of increasing the yield and tensile strengths. The presence of solid solution hardeners restrain the generation and motion of dislocations in a tensile test and hence should also restrain the generation and motion of dislocations under conditions of cyclic stressing and thus restrain their coalescence into the nucleus of a fatigue crack.

(b) The nature and distribution of the alloying element: Although alloy additions in general improve both the mechanical (tensile) properties and the fatigue properties of metals, the nature and distribution of the alloying element in the parent metal is an important variable. Alloy additions can result in two types of distribution of the added element in the parent element. If the alloy is soluble in the parent metal, a solid solution alloy is obtained which results in an increase in strength due to the changes in the lattice parameter resulting from the introduction of the foreign atom of a different size into the parent lattice. Solid solution hardening of this kind results in an impediment to dislocation motion in the material and hence in an improvement in tensile and fatigue properties.

A second form of alloy strengthening involves the addition of an insoluble or partially soluble alloying element to the metal to be strengthened. In such a situation strengthening is achieved by the impediment to dislocations presented by the dispersed particles of the insoluble second phase. This type of hardening, variously known as precipitation hardening, dispersion hardening, or second phase hardening is a close function of the type and distribution of the second phase. The common Al-1% Si alloy wires used in bonding represent good examples of the dispersion hardened system.

The Al-1% Mg alloy is a good example of the solid solution hardened system since all of the magnesium is in solution in aluminum.

In dispersion hardening the strength of the alloy is determined by the size and distribution of the dispersed phase. Consequently, if the distribution of the silicon in aluminum is changed in some way (for example, by heating) the strength of the wire will change. A more detailed discussion of this subject is presented in Appendix II.

3.3 THE CHOICE OF ALLOYING ELEMENTS

Considerable evidence has been accumulated on the effects of alloy additions to aluminum with particular reference to their mechanical properties. Figure 7 shows data taken from Dorn, et al[2] showing the effects of the addition of alloying elements on the stress-strain curves of aluminum. Some of these alloys are solid solution alloys with no precipitation or second phases present while others are precipitation hardened systems. No data on Al-1% Si is available to compare with this data. However, among the alloys shown the Al-0.082% Ge alloy is close to an Al-1% Si alloy in its mechanical behavior. This data clearly indicates the superiority of the Al-Mg and Al-Cu alloys in terms of high yield and tensile strengths. Figure 8 shows some accumulated fatigue data taken from the work of Riches, et al[3] of the same aluminum alloys as shown in Figure 7. This data clearly supports the contention that the Al-Mg and Al-Cu systems should be superior to

---

(2) Dorn, J. E., P. Pietroskowsky and T. E. Tietz; The Effect of Alloying Elements on the Plastic Properties of Aluminum Alloys; Trans AIME, 188, 933, (1950)

(3) Riches, J. W., O.D. Sherby and J. E. Dorn; The Fatigue Properties of some Binary Alpha Solid Solutions of Aluminum; Trans ASM, 44, 882 (1952)

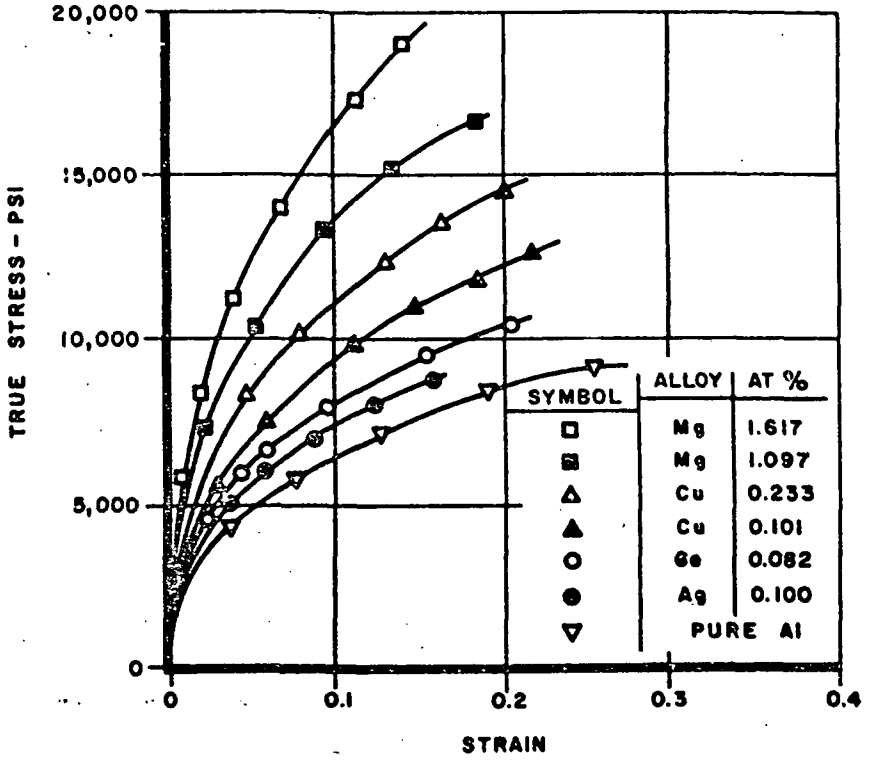

Figure 7. Stress-Strain Curves for Various Aluminum Alloys at 295°K (after Dorn ET AL (2))

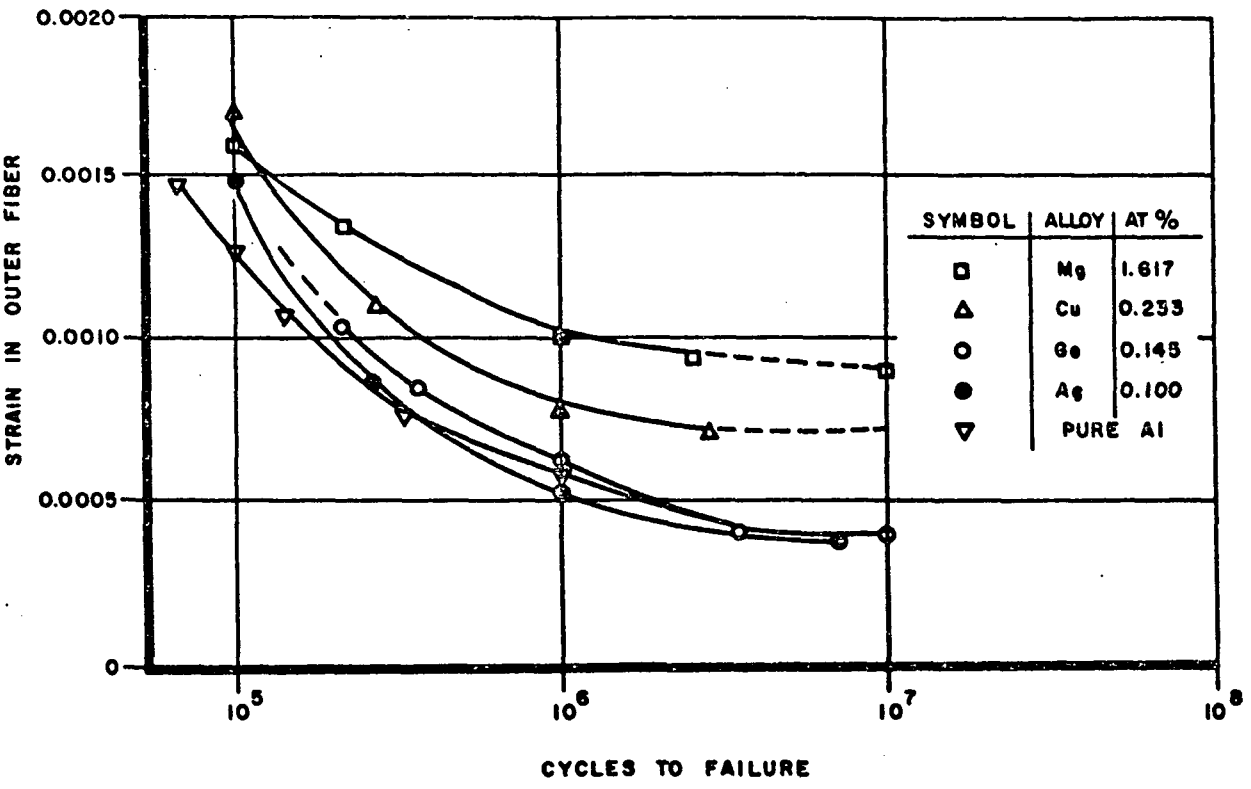

Figure 8. Effect of Alloy Additions on the Fatigue Properties of Alpha Solid Solutions of Aluminum at Room Temperature (after Riches ET. AL (3))

the dispersion hardened systems Al-Si with respect to the mechanical properties. Furthermore the solid solution system, (Al-Mg) is less susceptible to temperature induced changes in the properties than the Al-Si system. This will be discussed at greater length in a later section of this report. Based upon the obove mentioned considerations Al alloy wires 0.001 inch in diameter of the composition and as-received mechanical properties shown in Table I were obtained from different manufacturers.

Composition	Tensile Strength	% Elongation
Al - 1% Si	16-19 gms	2-5%
Al - 1% Mg	"	"
Al - 1% Cu	"	"
Al - 1% Mg - 0.5% Mn	"	"

TABLE I

The basic problem of the Al-1% Si systems is associated with its instability with respect to temperature. The silicon particles tend to grow with increasing temperature and large, uncontrolled silicon particles tend to reduce fatigue life by functioning as stress raisers which generate dislocations during fatigue and also by providing a low resistance path to the propogation of fatigue induced cracks. One solution to this problem is to use a solid solution hardened system without the presence of a second phase. The second solution is to prevent the growth of the dispersed phase (i.e. Si) by suitable alloy additions. The Al-Mg-Si system is one in which the second phase is a compound, Mg_2Si which is less susceptible to temperature induced coarsening. Attempts were made to obtain an alloy of Al-0.5% Si - 1% Mg in the form of 0.001-inch diameter wire. However no manufacturer

was able to supply this wire in 0.001-inch diameter form and the best efforts resulted in a 0.005-inch diameter wire. This wire was used to evaluate the effects of heat treatment on the structure and no attempts were made to evaluate its fatigue characteristics or to fabricate devices using this wire.

The Al-1% Mg - 0.5% Mn system is a combination solid solution hardened and dispersion hardened alloy. The magnesium in solid solution strengthens the aluminum and the manganese forms an insoluble Mn Al_6 phase which is dispersed in the form of fine particles throughout the Al-Mg solid solution. Consequently, both the effects of solid solution hardening and dispersion hardening are obtainable in this system. The essential portions of the phase diagrams of the alloy system studied are shown in Appendix III.

3.4 THE MECHANICAL PROPERTIES OF WIRES

In view of the close relation between fatigue properties and the tensile properties of wires, a study was made of the tensile properties of the various wires. The details of the testing procedures and the types of stress-strain curves obtained are shown in Appendix II.

Since the bonding (thermocompression) and packaging operations involve elevated temperatures (up to 400 to 500°C) the effects of high temperatures on the mechanical behavior were also investigated. Figure 9 presents cumulative data on the mechanical properties of Al-1% Si, Al-1% Cu, Al-1% Mg and Al-1% Mg 0.5% Mn alloys. The data shows the yield strengths (load at failure) as a function of the temperature of annealing. The wires were annealed for 15 minutes at each temperature in an inert ambient. Each data point represents the mean of at least six tests. The

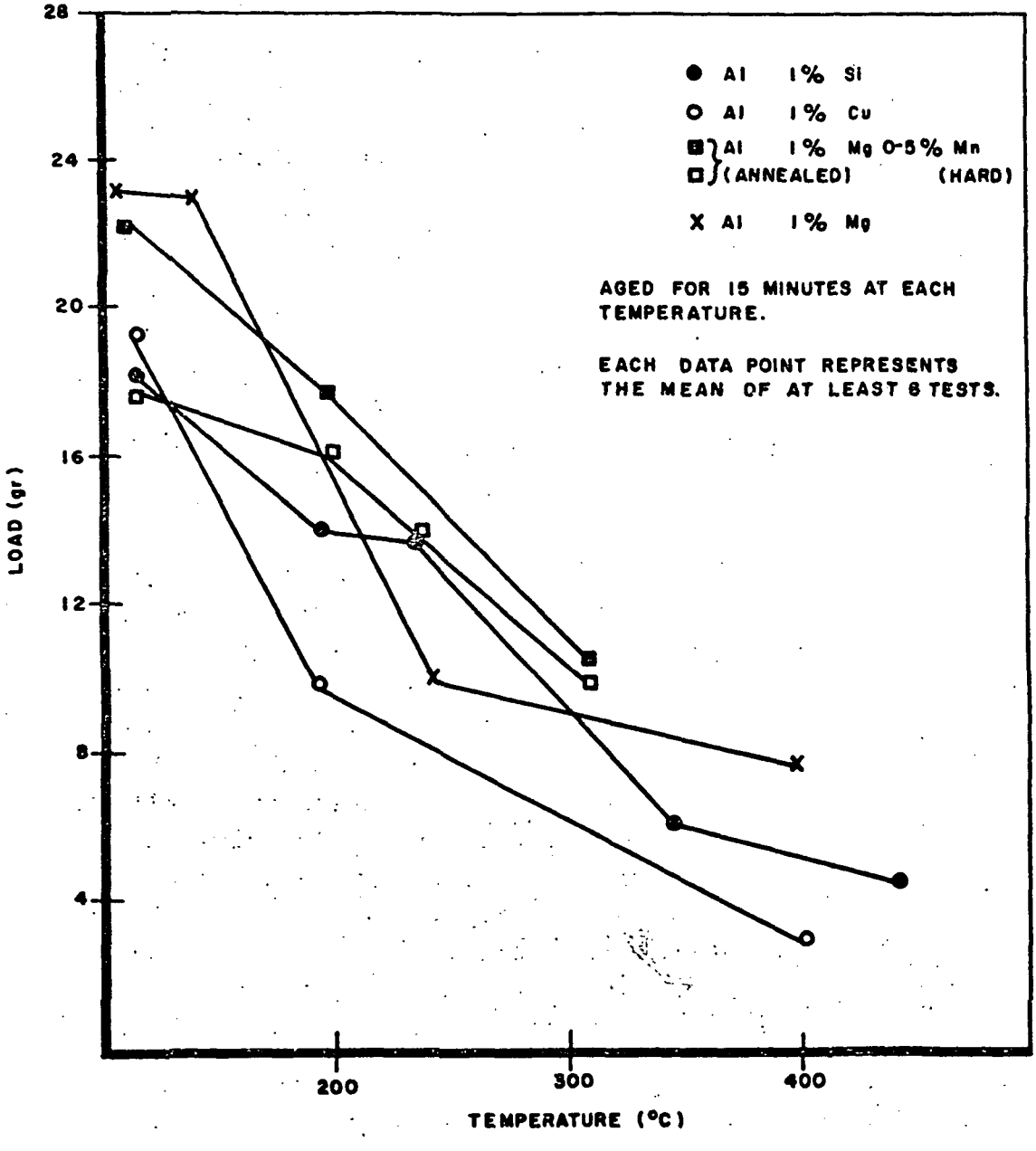

Figure 9. Breaking Strength as a Function of Annealing Temperature for Various Al Alloy Wires (0.001" Diameter)

Al-Mg and the Al-Mg-Mn wires show the best characteristics of retaining their strength at elevated temperatures when compared to the Al-Si wires. This behavior can again be attributed to the fact that the solid solution hardened alloys retain their strength better upon aging as compared to the dispersion hardened Al-Si alloys.

In general, the decrease in the tensile strength with elevated temperature aging follows a two-stage curve. The initial aging at low temperatures results in an abrupt loss in strength. With higher temperature aging, the slope of the curve tends to decrease. The initial stage of aging can be related to the annealing of the cold worked wire. Since the wire drawing operation involves considerable deformation of the wire, a large amount of cold work is retained in the wire.

The initial as-received strength of the wire in fact reflects this cold work to a large degree. It is thus possible for a wire manufacturer to furnish wire with a strength which varies over a wide range (from 6 to 20 gms for 1-mil wire). However, low temperature aging usually removes most of the cold work and drastically weakens the wire. Consequently, the strength of the starting material is not very relevant to obtaining a reliable bond. The second part of the aging curve generally relates to the agglomeration and growth characteristics of the dispersed phase in the aluminum. In general, the Si in Al-1% Si wire begins as a fine dispersion but with temperature it coarsens and hence contributes to the loss in strength. It is this strength, the dispersion imparted strength, of the wire that is important with respect to reliability factors such as power cycling. (See Appendix II for further discussion)

3.5 MICROPROBE ANALYSIS OF THE WIRES

The effect of the dispersed particle size on the mechanical behavior of Al-1% Si wires is discussed in Appendix II. To evaluate some of the other alloy systems with respect to the nature of the dispersion of any insoluble phases, a microprobe study was conducted of the wire after various aging treatments.

Figure 10, 11 and 12 show x-ray images of Al-1% Si, Al-1% Mg - 0.5% Mn and Al -0.5% Mg - 1% Si alloy wires. The Al-1% Mg system showed no changes in the x-ray images with elevated temperature aging and as such is not shown here.

The Al-1% Si alloy wire shows the presence of agglomerated Si particles when aged at high temperatures. The Al-Mg-Mn system remains essentially unchanged since the Mn Al_6 phase does not appear to grow with temperature. The Al-Mg-Si system shows the existence of the insoluble Mg_2Si phase, but this phase is relatively immune to temperature induced coarsening and consequently the particle size does not change with aging as shown in the microprobe analysis.

The results of this analysis coupled with the mechanical properties data indicate that a solid solution hardened alloy system or a stable dispersion hardened system is preferable to the Al-Si system for bonding applications. A factor to be considered in the results of the microprobe analysis is the resolution limits of this instrument. The microprobe is capable of a resolution of ~ 1 μm. Consequently second phase nonuniformities in the form of small clusters <1 μm in size cannot be detected by this instrument. Hence, the gross clustering of silicon in aluminum (Figure 10) indicates an advanced stage of clustering and growth of the silicon particles and the presence of many smaller clusters cannot be detected.

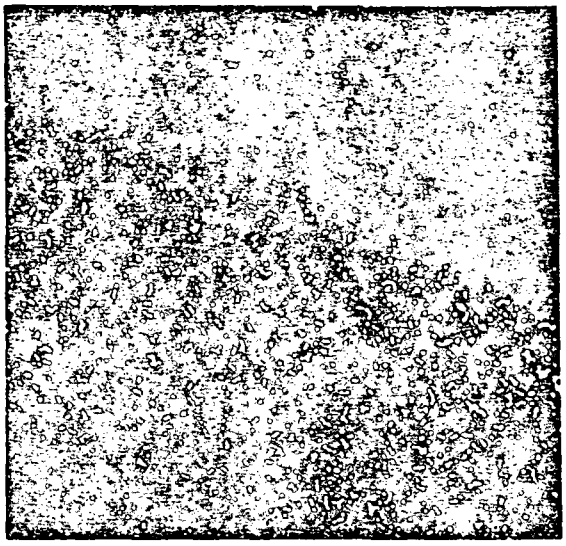

UNANNEALED

ANNEALED 200°C FOR
15 MINUTES

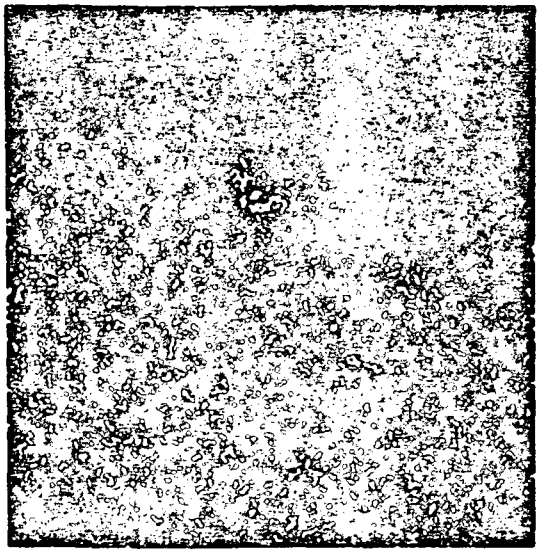

ANNEALED 300°C FOR
15 MINUTES

Figure 10. Si X-ray images of Al-1% Si Alloy Wires Subjected to Different Aging Treatments Showing the Agglomeration of Silicon.

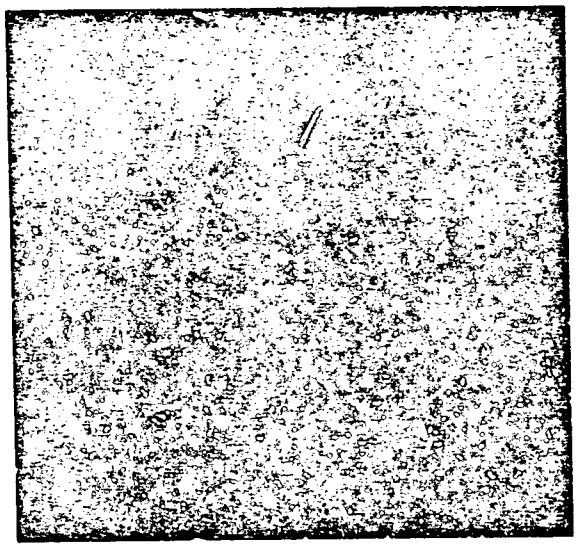

Mg

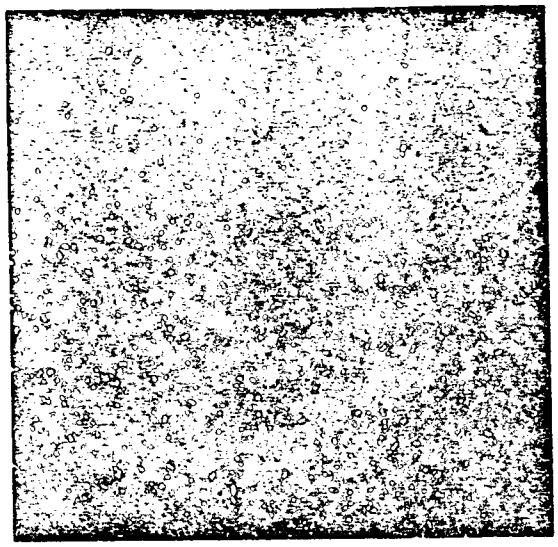

Mn

ANNEALED 300°C FOR 15 MINUTES

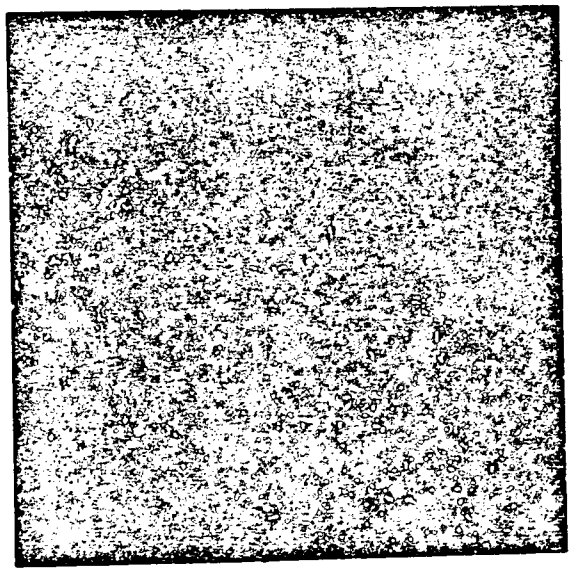

Mg

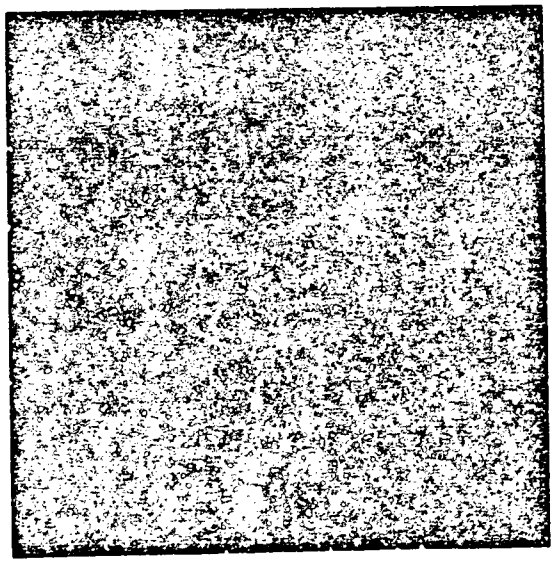

Mn

ANNEALED 300° FOR 15 MINUTES

Figure 11. Mg and Mn X-ray Images from Al-1% Mg-0.5% Mn alloy wire

9811-11-1

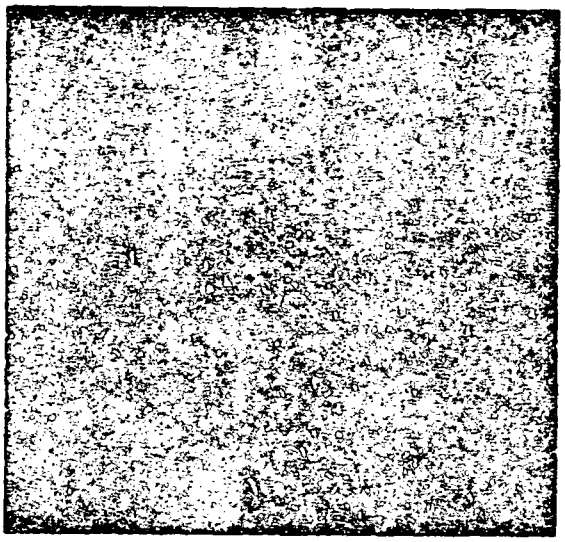

Mg

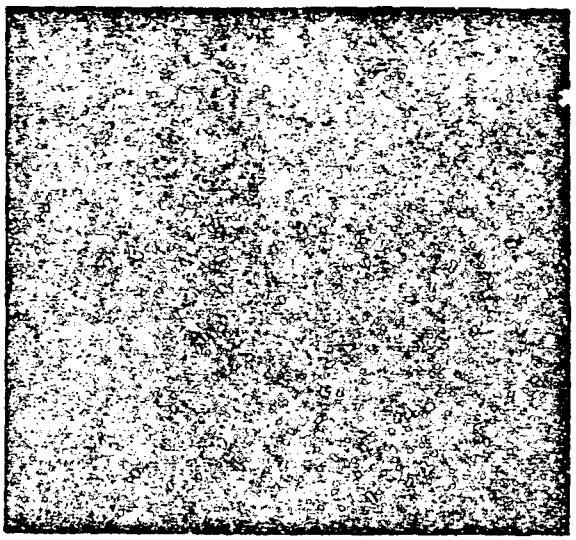

Mn

UNANNEALED

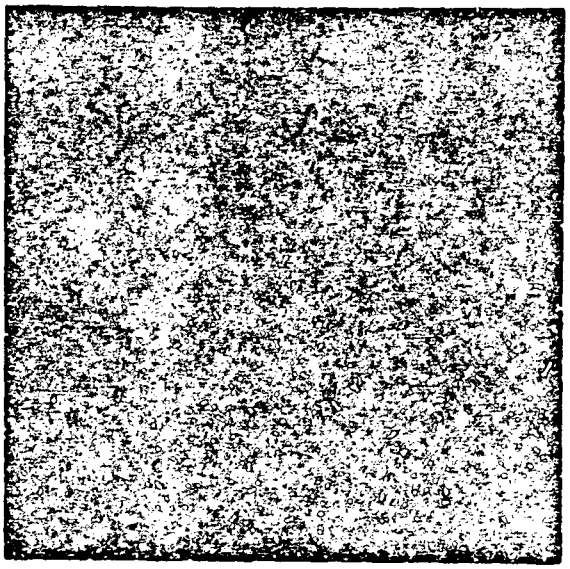

Mg

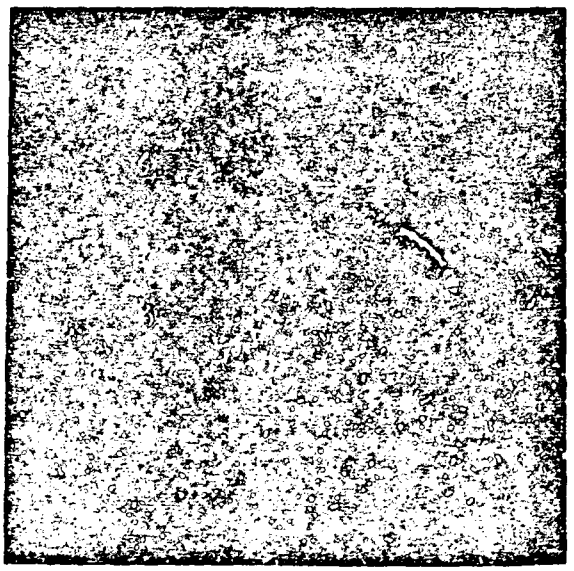

Mn

ANNEALED 200°C FOR 15 MINUTES

Figure 11. (Cont'd.)

9812-11-1

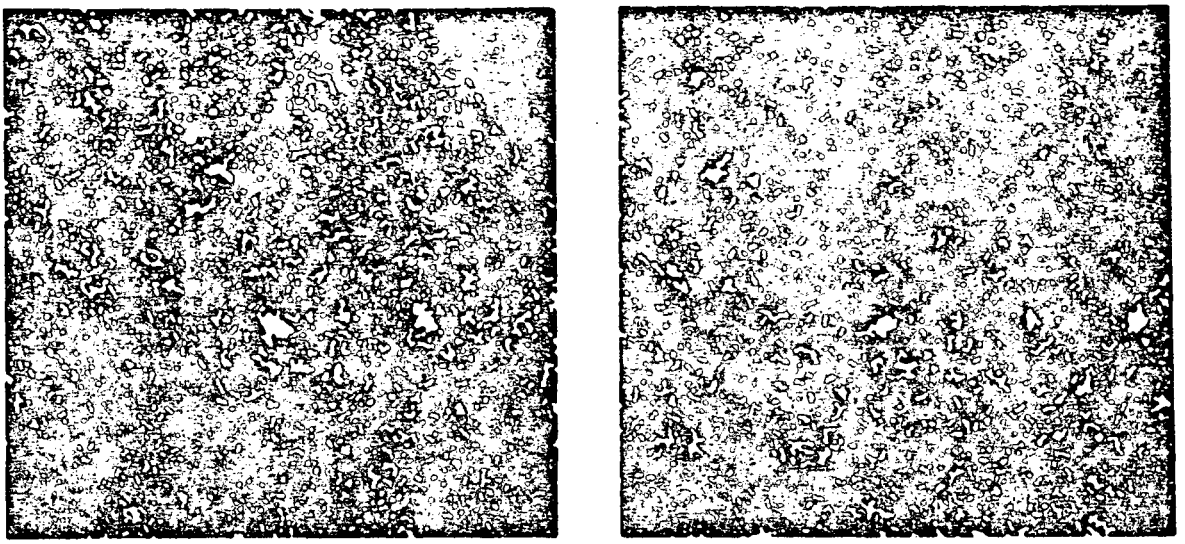

Mg Si

UNANNEALED

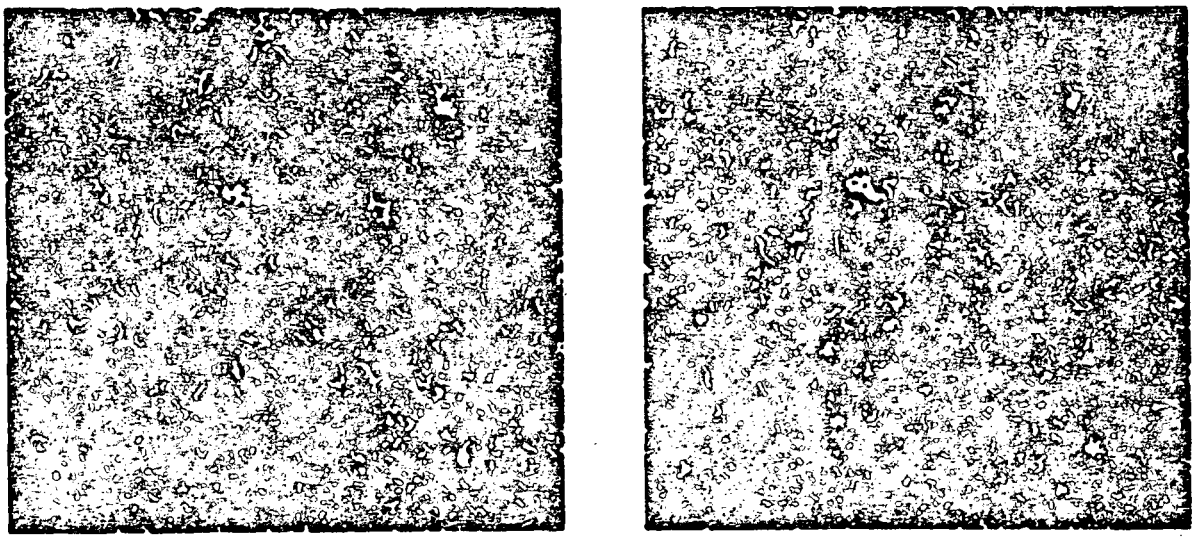

Mg Si

ANNEALED 200°C FOR 15 MINUTES

Figure 12. Mg and Si X-ray Images from Al-1% Mg - 0.5% Si Alloy Wire

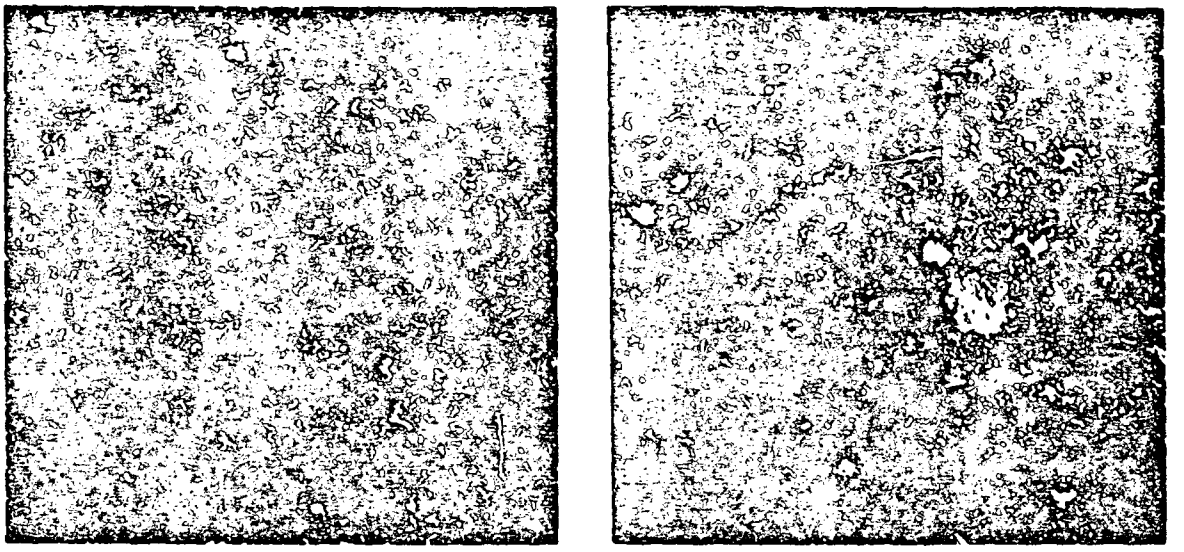

Mg Si

ANNEALED 300°C FOR 15 MINUTES

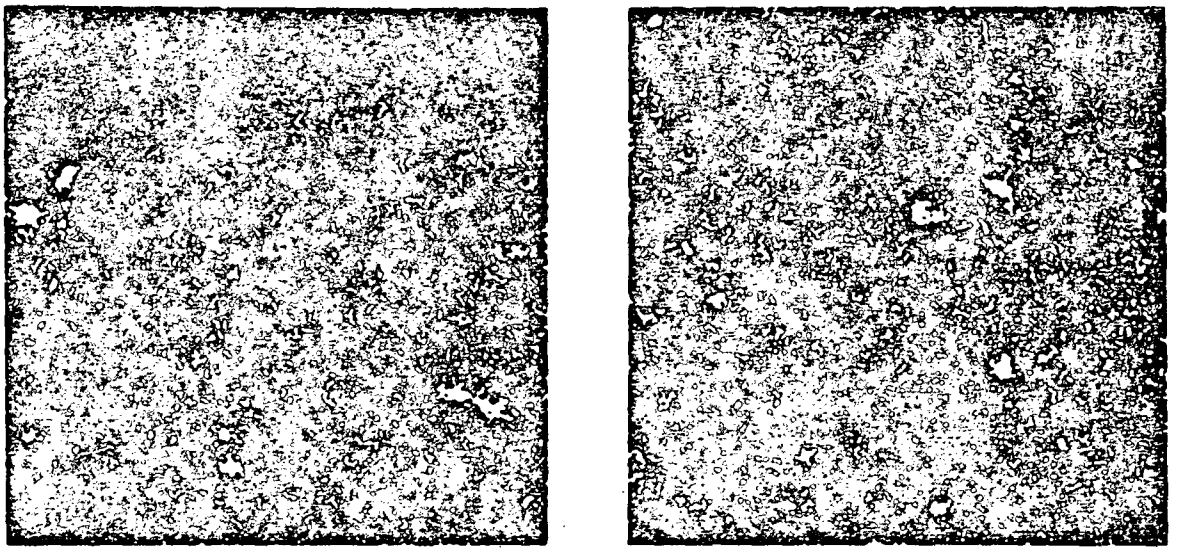

Mg Si

ANNEALED 400°C FOR 15 MINUTES

Figure 12. (Cont'd.)

3.6 OPTIMIZATION OF THE ULTRASONIC BONDING PROCESS

To understand the conditions required for optimizing the ultrasonic bonding process, it is first necessary to understand the steps involved in producing an ultrasonic bond. A typical design for an ultrasonic wire bonder is shown in Figure 13. The vibrator is an ultrasonic transducer which typically operates in the range of 50 to 60 kHz. The coupling of the wire to the vibrator is accomplished by the use of a tungsten carbide bonding wedge. The bonding process begins when the wedge is lowered onto the wire which in turn is forced against the metallization on the bonding pad. The weight on the tool deforms the wire and permits locking between the edges of the wedge and the deformed wire.

The bonding process begins at the interface between the wire and the metallization. Both aluminum surfaces to be joined are atomically rough and are covered by a tenacious oxide 20 to 100Å thick. In addition to normal surface irregularities, aluminum metallization will contain annealing hillocks (Figure 14) up to 1 micron high. These hillocks result from compressional stresses in the aluminum caused by thermal expansion differences between aluminum, SiO_2, and silicon during temperature excursions such as die bonding. Aluminum wire can contain drawing marks several thousand angstroms deep. When the surfaces are brought together under pressure, the initial contact area is small because only the high points make contact. These hills can deform only moderately because the aluminum work hardens and the normal stress decreases (as the contact area increases).

The ultrasonic vibration is applied and friction between surfaces locally heats the interface over several hundred degrees while the aluminum away from the interface remains cool.

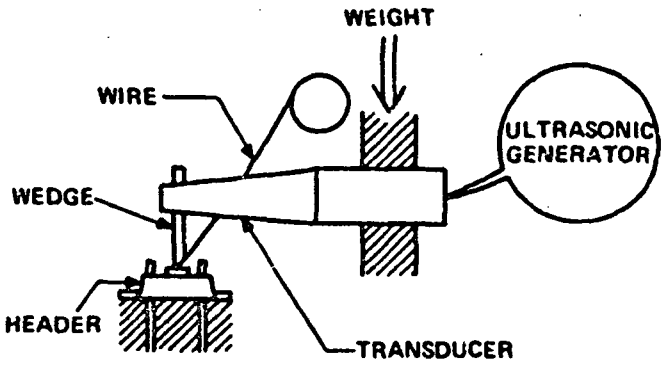

Figure 13. A Simplified Sketch of an Ultrasonic Wire Bonder

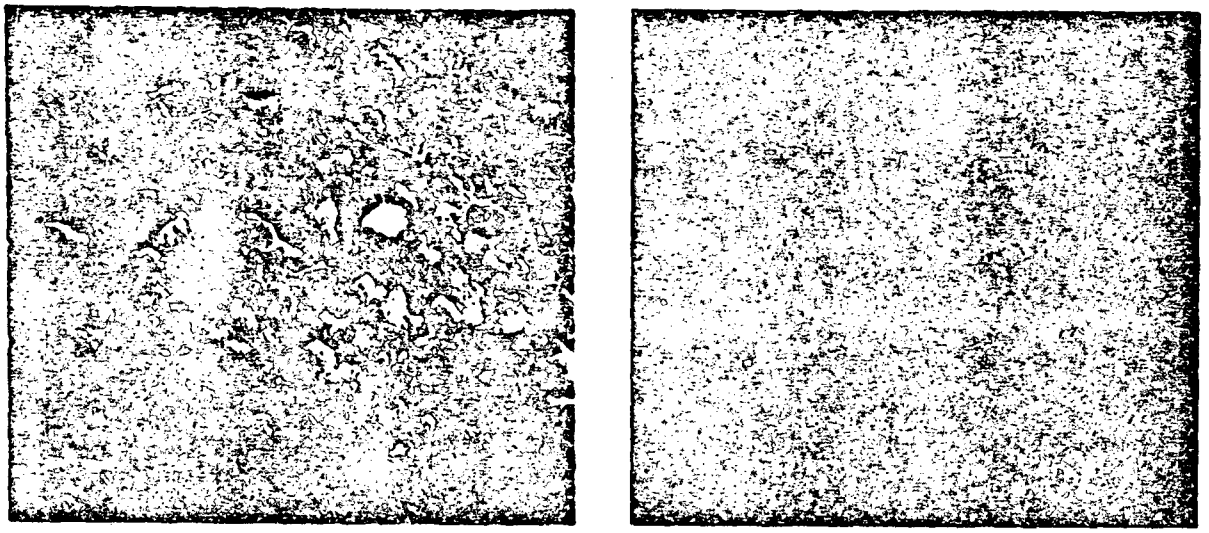

VACUUM – 5×10^{-8} TORR

VACUUM – 5×10^{-5} TORR

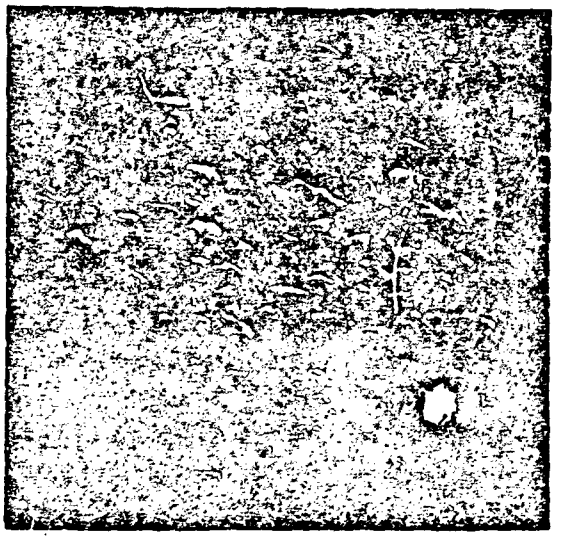

VACUUM – 1×10^{-3} TORR

Figure 14. Annealing Hillocks in Deposited Aluminum under Different Conditions of Deposition Vacuum.

Because the aluminum alloys used for wire soften dramatically at elevated temperatures (Figure 15), further local deformation proceeds at the interface increasing the contact area. The ultrasonic vibrations smear the surface oxides and contamination exposing fresh metal surfaces which bond by cohesion. In this manner, a metallurgical bond can be made between aluminum surfaces in tens of milliseconds with the heavy deformation zone limited to the interfacial area. Further vibrations once the bond is made stress the bonded area and, if allowed to continue, can begin to rupture it by fatigue.

Many variables affect the ultrasonic bonding process including the mechanical properties and surface condition of the wire, the mechanical properties and surface condition of the metallization, ultrasonic power, dwell time, pressure, resonance of the system, tool geometry and wear, and alignment. The first two variables are material variables and have been studied only briefly in the past, even though they can have a dramatic impact on the strength of the wire bond. Because of their potential importance, these two variables were extensively studied in this program and results are reported in separate sections of this report. The remaining variables are machine variables and these have been extensively studied and optimized in the past by many investigators. They were therefore not studied separately but rather optimized for each material studied using the procedure described in the following paragraphs.

The bonding was performed on a West Bond "mini" bonder. The machine was aligned so all the energy from the ultrasonic generator was transferred to the tip of the wedge. The machine variables -- dwell time, power, and pressure -- were then optimized for each spool of wire with differing tensile properties by keeping two of the variables constant while varying the third.

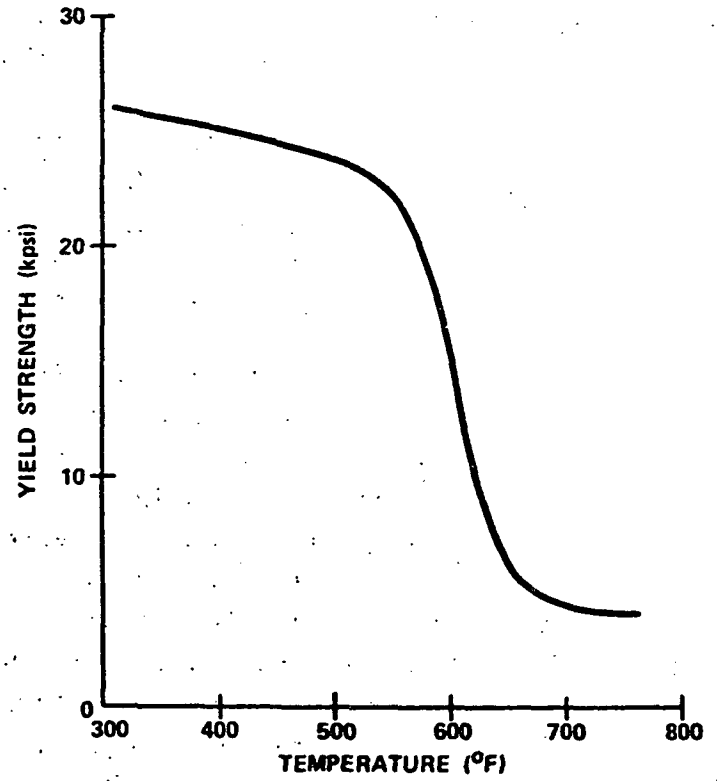

Figure 15. Yield Strength as a Function of Temperature for Aluminum

An example of this optimization procedure is shown for an Al-1% Si wire with an 18.7 gram tensile strength. Figure 16 shows the effect of varying the power setting on the pull strength. It is seen that the bond strength is optimized at a setting between 2.5 and 2.8. Below these values, the bonds are weaker and tend to lift due to insufficient bonding. Figure 17 shows the effect of needle weight setting on pull strength. The bond strength is optimized at 26 gram needle weight setting. Figure 18 shows the effect of time setting on bond strength and it is seen that a setting of 3.5 is optimum. Thus, for this wire of 18.7 gram tensile strength, the optimum machine settings are: power setting - 2.7, time setting - 3.5, needle weight - 26 grams.

This procedure must be repeated for each wire of differing tensile properties. If not, poor bonds can result as shown in Figure 19. This figure shows bonds made at the machine settings described in the preceding paragraph. Figure 19 (a) is a bond made with 1-mil diameter 18.7 gram tensile strength wire which had a narrow bond width (1.4 mils) and excellent wire pull. Figure 19 (b) is a bond made with 1-mil diameter 14.5 gram tensile strength wire which had excessive deformation (2.7 mil bond width). This resulted in low wire pull strength with the failure mode being heel breaks. For these lower tensile strength wires, the needle weight and ultrasonic power should have been reduced to optimize the bonding.

3.7 THE MECHANICAL PROPERTIES OF THE METALLIZATION

As discussed in section 3.6 among the factors that affect the integrity of the ultrasonic bonding operation are the mechanical properties and surface quality of the thin film metallization on the die. As a part of this program, some studies were made on these factors.

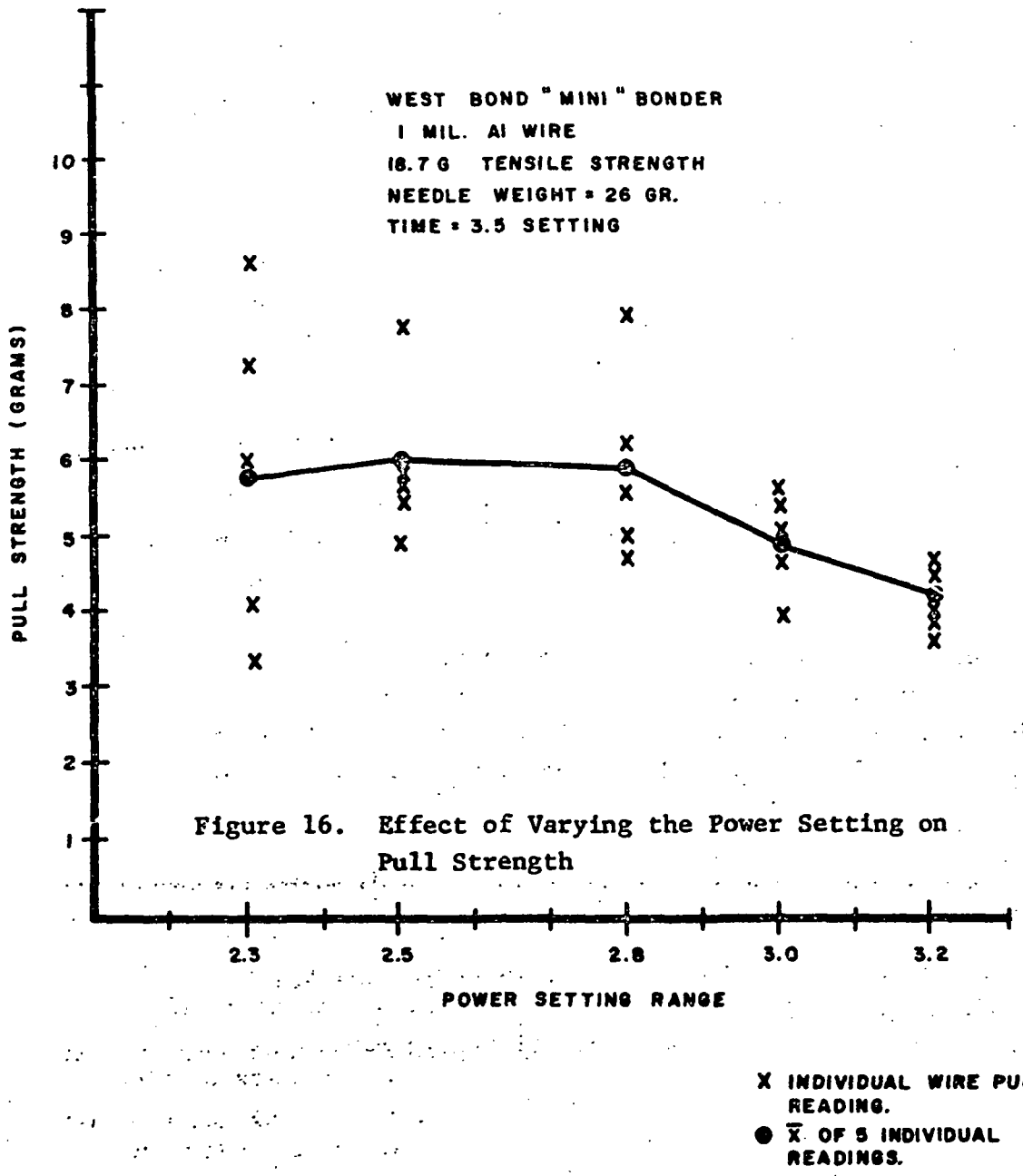

Figure 16. Effect of Varying the Power Setting on Pull Strength

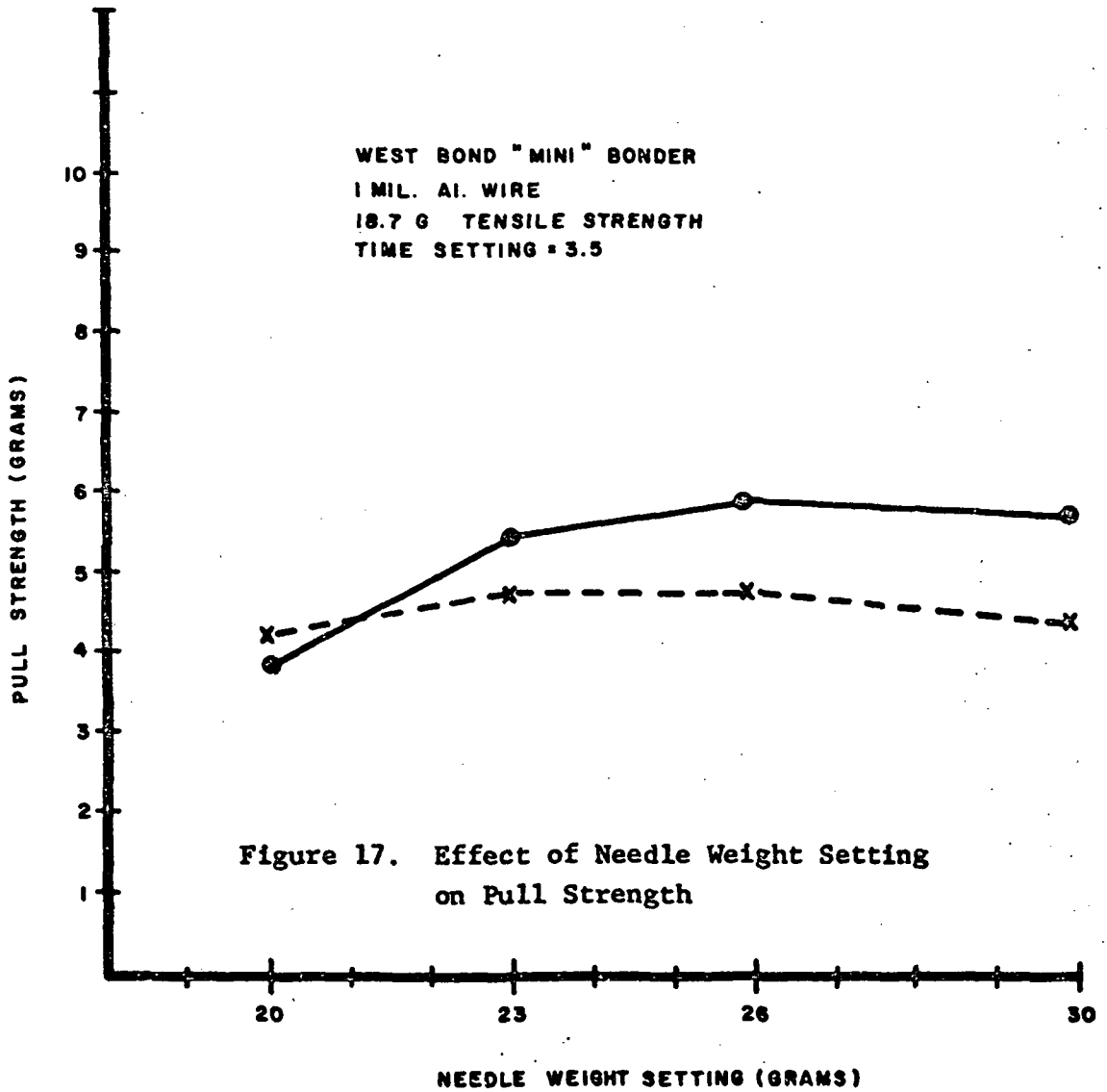

Figure 17. Effect of Needle Weight Setting on Pull Strength

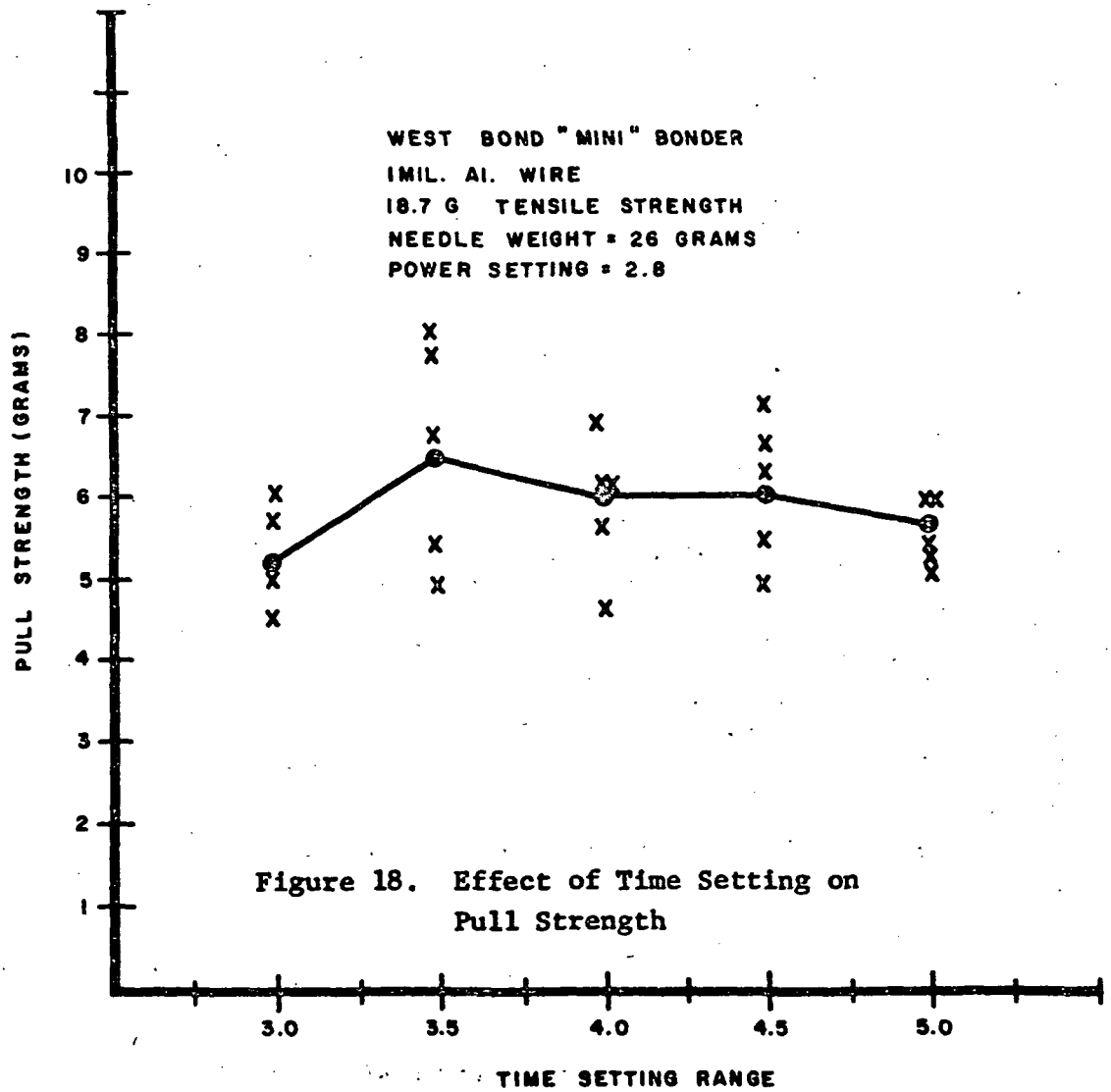

Figure 18. Effect of Time Setting on Pull Strength

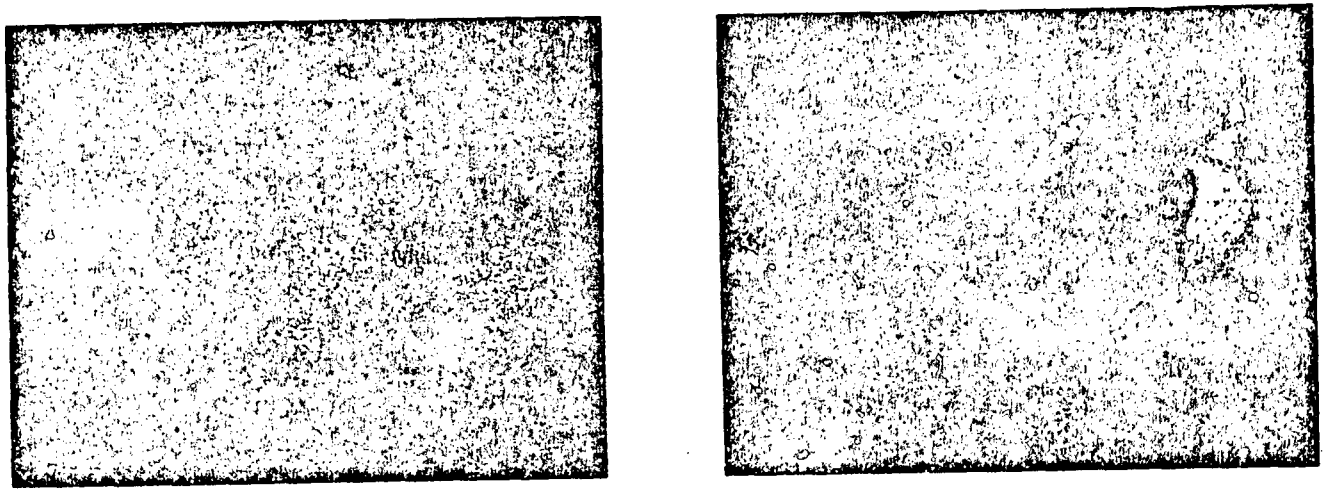

(a) (b)

Figure 19. Bond Deformation when using a High Tensile Strength Wire (18.7 gms) Shown in A and a Low Tensile Strength Wire (14.5 gms) Shown in B

The mechanical properties of evaporated aluminum films were studied by the technique of applying a biaxial stress to the film. This was achieved by the construction of a special apparatus which enabled the application of a biaxial stress to the thin film and the measurement of the elastic and plastic strains introduced in the film as a result of the applied stress.

Films of aluminum approximately 1 micron in thickness were evaporated on silicon substrates. The vacuum, substrate temperature and the evaporation rate were varied in order to observe the effects of these variables on the mechanical properties.

Circular holes approximately 0.5 cm in diameter were chemically etched in the silicon beneath the aluminum films using photolithographic techniques and protecting the aluminum from the etchant. This resulted in the aluminum films streched over circular holes in the silicon. Pressure was now applied to the aluminum films by the use of a specially constructed apparatus consisting of a metal block with a circular hole of the same diameter as the holes cut in the silicon. Pressurized air could be conveyed through the hole and made to come into contact with the aluminum film covering the hole in the silicon. This was made possible by suitably clamping the silicon over the metal block with the hole in the silicon conciding with the hole in the metal block. With the application of pressure to the aluminum, the film bulges upwards due to the deformation introduced into the film by the action of the pressured air. The degree of bulging was measured by a micrometer screw-gage which was brought into contact with the bulging film after each incremental application of pressure. The pressure applied was measured by means of a pressure gage. Figure 20 shows a schematic of the apparatus and the technique used to measure the strength of the thin films.

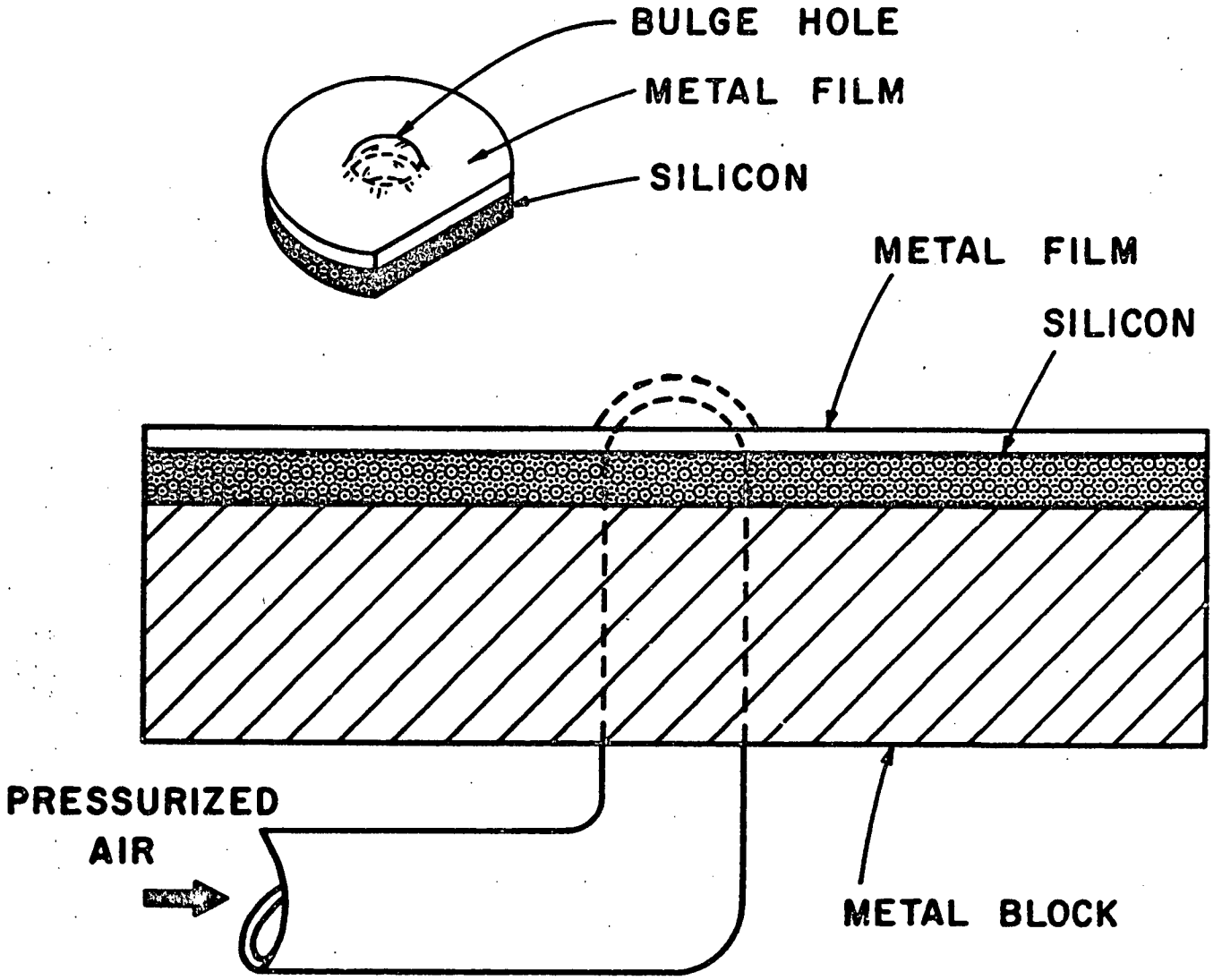

Figure 20. Schematic of Biaxial Bulge Tester

9822-11-1

Stress-strain values were calculated on a computer using the following relations:

$$\text{Stress } \sigma = \frac{PR^2}{4Ht}$$

$$\text{Strain } E = \frac{H^2}{R^2}$$

where P is the applied pressure, R is the radius of the hole in the silicon, H is the height of the bulged film and t is the film thickness which was measured by intereferometry.

Figure 21 shows typical stress-strain curves of different aluminum films with the evaporation conditions shown.

Dice from wafers with different types of Al films were suitably mounted on headers and thermocompression bonds made using 1 mil Al - 1% Si wires. The bonding was done in a production area under typical production conditions. Wire pull data were obtained for all the types of metallization studied. Figure 22 shows a plot of the bond pull strength as a function of the tensile strength (the maximum stress in Figure 21) of the substrate metallization.

Although some effects of film strength on the wire pull strength were observed with an increase in the pull strength with increasing strength of the substrate metallization, the most significant result was the effect of the wire strength on bond pull strength. Furthermore, since the mechanical properties (the tensile strength) of the films shown in Figure 21 are essentially the same for different evaporation conditions, the present indications are that the strength of conventionally obtainable aluminum films should have little effect on bond pull strength or reliability, and the over-riding factor is the mechanical behavior of the bonding wires.

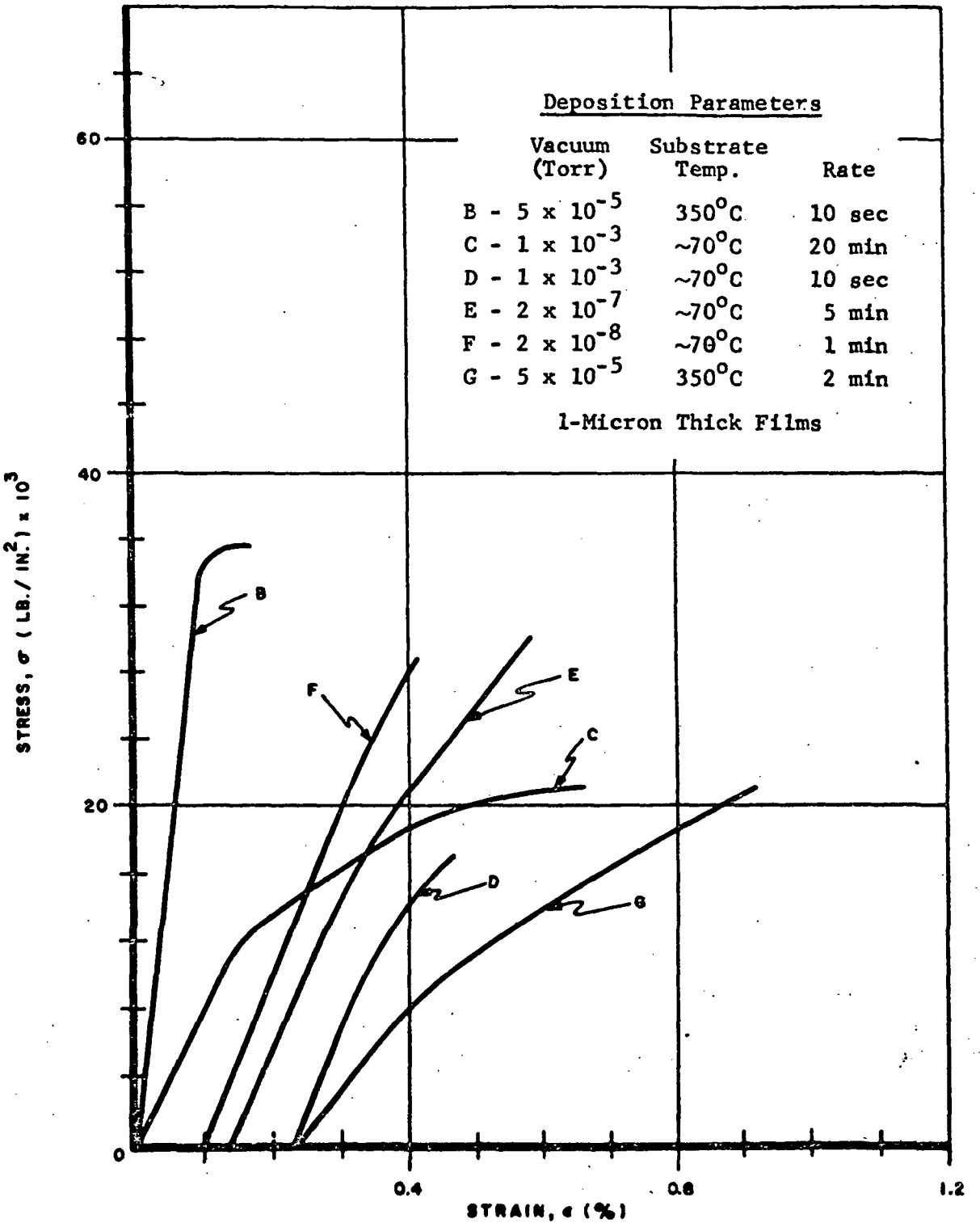

Figure 21. Stress-strain Curves of Different Aluminum Films

9823-11-1

Figure 22 shows that the wire with a 16 gm tensile strength results in consistantly high pull strengths when bonded to metallization of different yield strengths. Both the 13.8 gm and the 19.8 gm tensile strength wires by comparison form weaker bonds. The soft wire results in excessive deformation of the bond with the resultant reduction in the pull strength (see Figure 19 (b)). The high strength wire (19.8 gm) also results in a low pull strength. This can be attributed to the fact that the high strength of the wire is a result of the large degree of cold work retained in the wire. The cold work is introduced during the wire drawing operation and has not been annealed out. During bonding further work hardening of the wire results with the attendant embrittlement of the heel of the bond. A hand wire is also more susceptible to the formation of microcracks during bonding.

A wire which is both strong and ductile has the best properties for obtaining good bonds which are not excessively deformed and are sufficiently free of work hardening to resist crack formation.

3.8 ACCELERATED FATIGUE TESTING

2N2222 devices were built using the different aluminum alloy wires investigated in this program. Both thermocompression and ultrasonic bonding was employed to form the bonds. The bonding conditions and controls used were discussed in a previous section of this report. The wire bonds were tested on the accelerated fatigue testing apparatus. The raw data obtained is shown in Table II. Figure 23 presents the S-N (fatigue) curves for the different alloys investigated (with the exception of the Al-Mg-Mn alloy wires). At any specific level of deflection the Al-Mg and Al-Cu alloys will result in a longer life when compared to the Al-Si wires. At deflections below 4×10^{-4} inch which represent

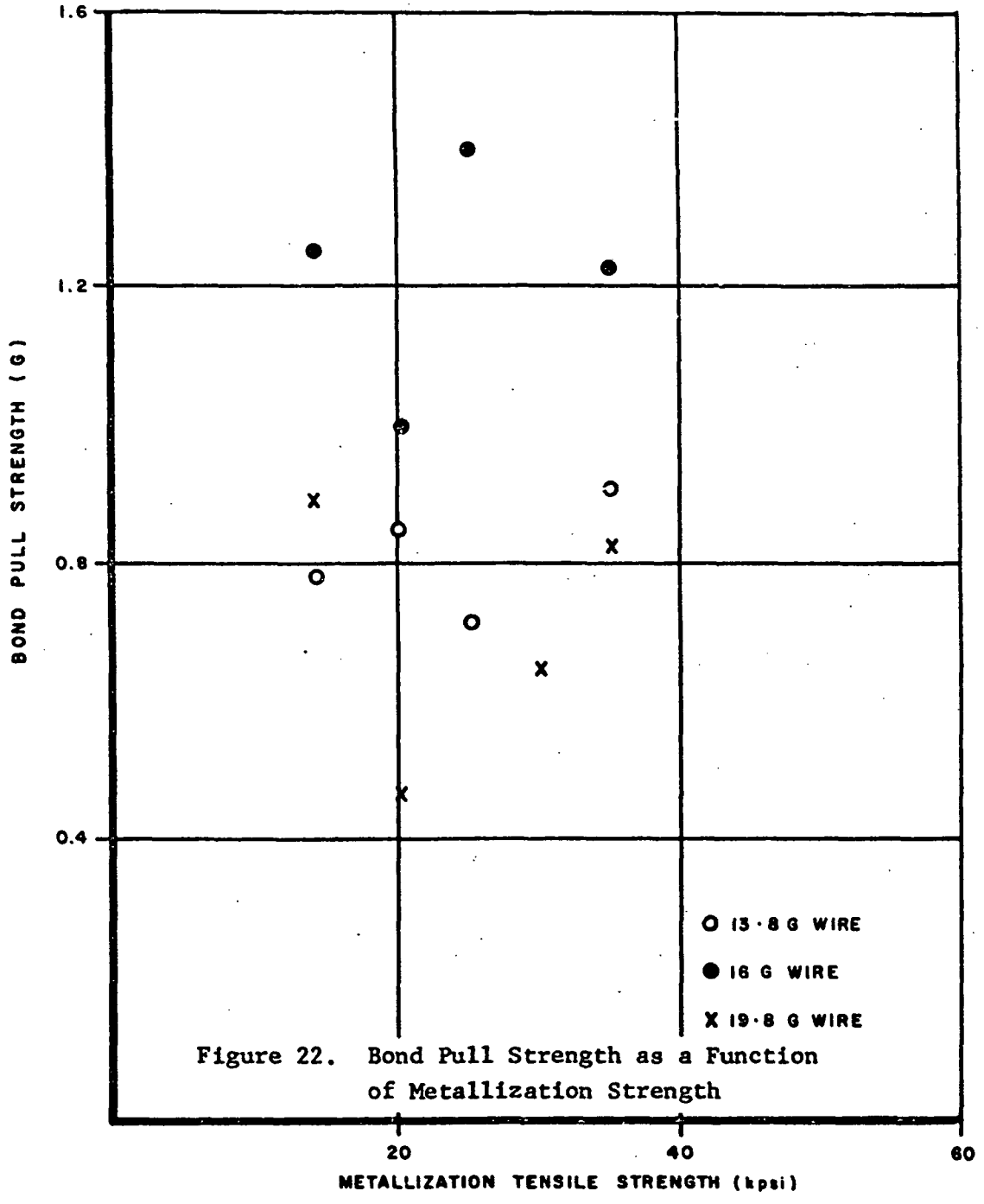

Figure 22. Bond Pull Strength as a Function of Metallization Strength

9824-11-1

Al - 1% Si (Thermo-Compression)		Al - 1% Si (Ultrasonic)		Al - 1% Cu (Ultrasonic)		Al - 1% Mg (Ultrasonic)	
Deflection $x10^{-4}$ in	Cycles to Failure $x10^3$	Deflection $x10^{-4}$ in	Cycles to Failure $x10^3$	Deflection $x10^{-4}$ in	Cycles to Failure $x10^3$	Deflection $x10^{-4}$ in	Cycles to Failure $x10^3$
	0.1		0.2		0.1		1.5
11.4	0.3	7.7	0.3	10.4	0.3	10.4	1.7
	0.4		0.5		0.5		1.8
	1.0		1.4		1.0		2.2
	1.2		2.4		1.1		
	1.4		2.6		3.6		3.2
7.6	1.6	5.8	3	7.6	3.8	6.4	3.6
	1.9		3.4		4.		3.7
	2.2				4.4		4.0
	1.6		24				4.2
5.8	1.9	3.8	25		12		24
	2		27	6	14		25
	2.4		28		15	5.2	27
4.8	2.6		29		16		28
	3		38		17		
	3.5		39		18		
	3.7	3	41		44		
	4			3.4	45		
	2 2				47	4.4	>50
	2 3						
2	2 4						

TABLE II

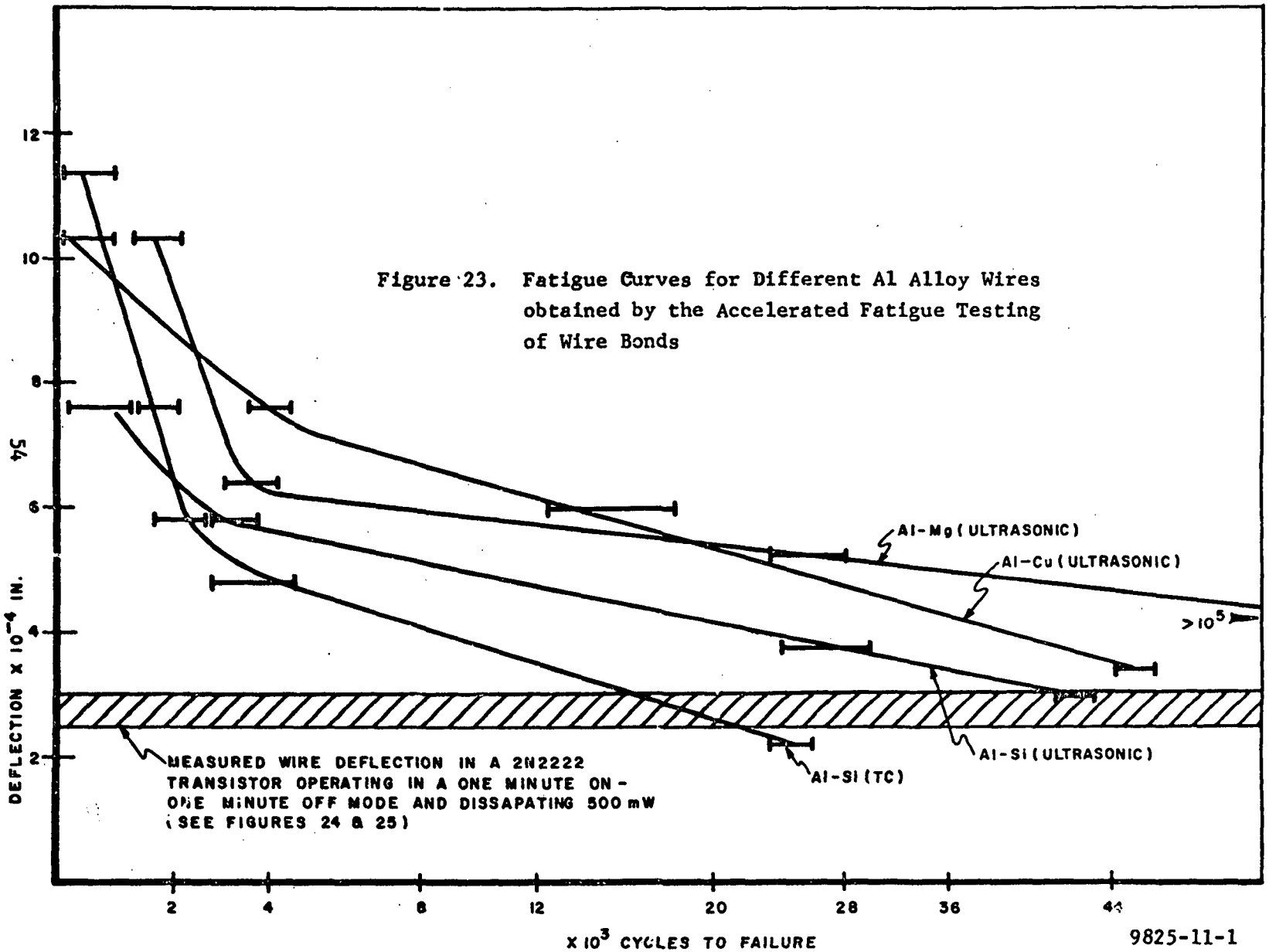

Figure 23. Fatigue Curves for Different Al Alloy Wires obtained by the Accelerated Fatigue Testing of Wire Bonds

typical values of the deflection (between 2 and 4 x 10^{-4} inch) experienced by the wire during the on-off operation mode the Al-1% Mg wire did not fail and the tests were discontinued once the number of cycles had reached approximately 10^5.

As discussed in the experimental procedure section, attempts were made to measure the degree of deflection experienced by the wire during operation by operating the device in an on-off mode in the SEM. Figures 24 and 25 show pictures of the wire bond at the heel, and at a distance midway between the heel and the post respectively. Photographs show the position of the wire during the off (Figure 24)and on (Figure 25) cycles. The sketch shows the deflection obtained during this operation. Within the limits of experimental error the maximum deflection observed at the center of the wire is 0.25 to 0.3 mils (2 to 3 x 10^{-4} inch). The deflection is less at the heel of the bond and near the post as would be expected. This measurement obtained in the SEM may not be very accurate in view of the fact that the heat transfer characteristics of the device and the package are not exactly identical when the device is operated inside the SEM and outside the vacuum environment of the SEM. However, the data are sufficiently accurate to use in conjunction with the S-N curves of Figure 23 to obtain the lifetimes of the different wires when operated in the 1-minute on and 1-minute off mode. The horizontal band shown in Figure 23 represents the deflection experienced by the wire and the intersection of this band with the fatigue curves give the corresponding values for the number of cycles each wire will last before failure. The Al-Mg wire has a fatigue curve which does not intersect the horizontal band for the data presented indicating that wire bonds made with Al-1% Mg wires should last $>10^5$ on-off cycles without failure.

Figure 26 shows the fatigue curves obtained for thermocompression and ultrasonic bonds using Al-1% Si wire. It is

Figure 24. Wire with Device Turned Off.
Micrographs at the right are of
the center portion of the bond

9826-11-1

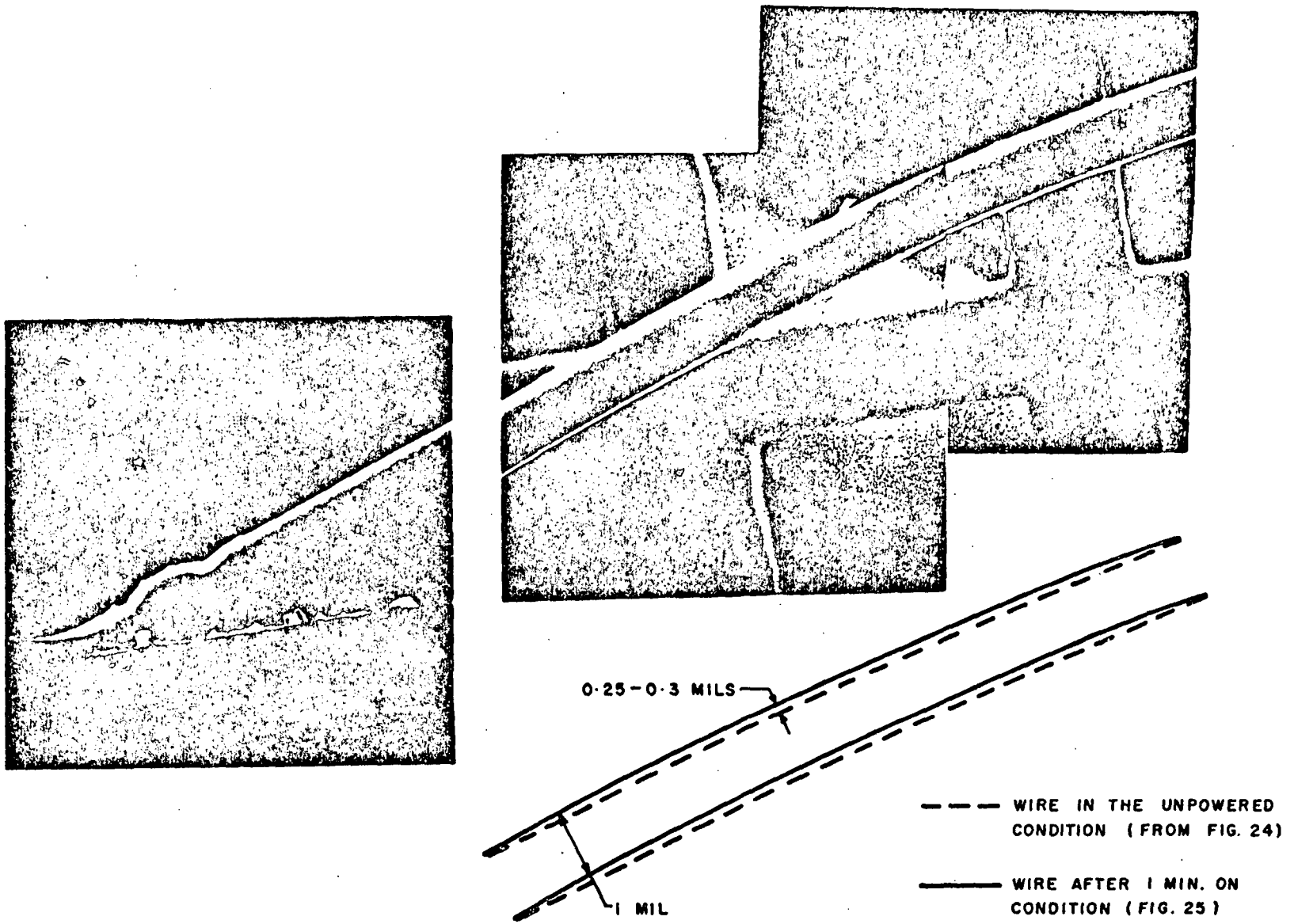

Figure 25. Wire in the On Condition (Power Dissipation - 500 mW) One Minute On

9827-11-1

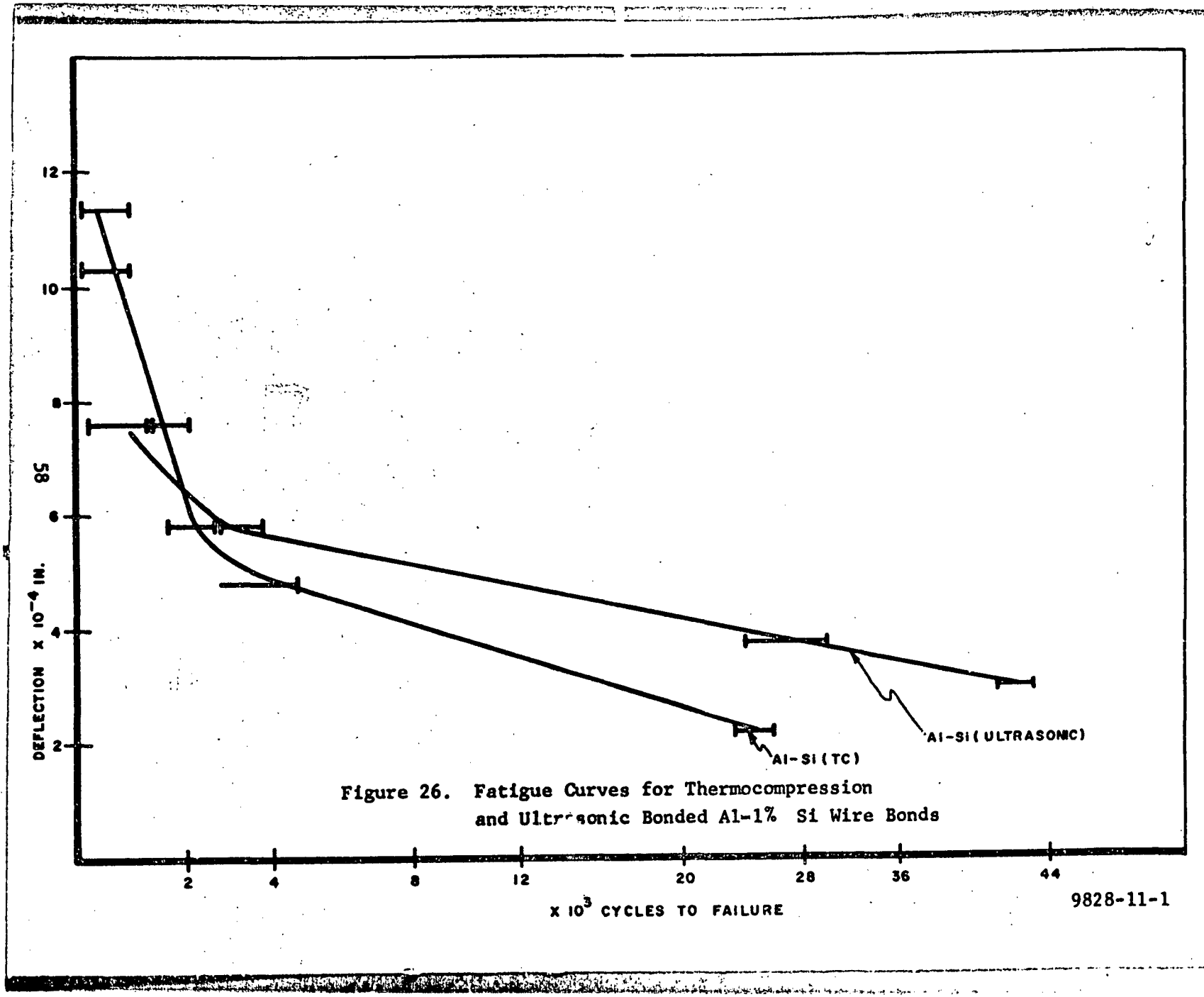

Figure 26. Fatigue Curves for Thermocompression and Ultrasonic Bonded Al-1% Si Wire Bonds

evident that ultrasonic bonding results in an overall increase in the fatigue life of the bond. A short discussion on the possible reasons for the superior fatigue behavior of ultrasonic bonds will be presented.

The thermocompression bonding operation involves a combination of temperature and pressure being applied to the wire whereas ultrasonic bonding does not involve temperature. At elevated temperatures, the aluminum wire has a tendency to work harden more rapidly due to the rapid motion and multiplication of dislocations whereas at room temperature the deformation of the wire associated with ultrasonic bonding results in a bonded region (the bond and the heel of the bond) which is in a less work hardened state.

Fatigue of the wire introduces more dislocations into the material and hence causes fracture. In the case of the thermocompression bonds, the more work hardened state of the bond results in a reduction of the fatigue life as compared to the ultrasonic bonds.

Another factor that results in a better bond when ultrasonic energy is used to make the bond is the fact that ultrasonic bonding results in a smaller amount of deformation of the wire when compared to TC bonding since during ultrasonic bonding most of the deformation is confined to the interface between the wire and the substrate metallization whereas in TC bonding the entire wire is deformed.

Some of the essential similarities and possible differences between the accelerated fatigue test results and test results obtained by operating the devices in the on-off mode (life tests) will be discussed in order to ascertain the degree of reliability that can be placed on the data obtained with the accelerated testing apparatus.

(a) The direction and magnitude of motion of the wire is the same in both methods of testing of the wires. Since the motion introduced at the heel by the differential thermal expansion of the aluminum and the package is the cause for fatigue failure it is immaterial whether the motion is introduced during device operation or by means of the accelerated test.

(b) The accelerated test is conducted at room temperature whereas the wire does experience high temperatures (approximately 100°C) during operation. However, this factor only makes the accelerated test more drastic since the damage in the form of piled up dislocations introduced by flexing can be partially annealed out at the high temperatures during the on-off tests and hence result in an increased lifetime as compared to the lifetime obtained by the use of the accelerated tester. This indicates that the accelerated fatigue data is on the conservative side.

(c) The mounting techniques employed for testing the wire bonds in the accelerated tester involve some degree of handling of the wire. It is therefore possible to introduce some damage to the heel of the bond. However, in such situations the fatigue life is drastically reduced and does not conform to the data obtained on undamaged bonds. Such non-ideal tests were discarded and tests repeated until reproducible values were obtained.

(d) The accelerated fatigue testing apparatus has been designed to apply a flexing load to the wire. However it has been found that a small degree of pull (tensile load) is also experienced by the wire when tested on this machine. This would again aggravate the stress conditions and result in an earlier failure of the wire bond. This makes the accelerated test more drastic than the operational life test and as such is a desirable condition.

In summary, although good correlation between the accelerated tests and operational life tests has been obtained it must be emphasized that the accelerated fatigue data should be used only to gauge the relative properties of wire bond materials. These data are not considered to be exactly analogous to data obtained on life tests. Accelerated fatigue testing is a quick means of evaluating different wire bond systems for their relative efficiencies in improving reliability and increasing lifetimes.

3.9 WIRE DRESSING EFFECTS

Increased height of the wire loop has been shown mathematically to decrease the degree of motion of the wire at the point of maximum flexure[4]. Based upon this analysis it has been suggested that an increased loop height be used to increase fatigue lifetime.

With respect to fatigue, the important consideration is the degree of motion at the heel of the bond and more specifically the change in the contact angle ($\phi - \phi_o$) that occurs during power cycling. An analysis of the effect of h_o/d_o on ($\phi - \phi_o$) has been made where h_o/d_o is the ratio of the loop height to the loop length of a wire bond and the contact angle is the angle between the wire bond and the metallization on the die. This analysis shows that with increasing h_o/d_o i.e. increasing loop height, the change in the contact angle that occurs when the wire expands during the on-cycle of the device decreases. However this decrease is most rapid when h_o/d_o is < 0.1. Beyond ~ 0.1 further increase in h_o/d_o changes ($\phi - \phi_o$) by a very small value ($\leq 0.5^o$) and the change is insignificantly small for $h_o/d_o > 0.15$. In practice it is physically impossible to produce bonds with small enough loop heights to obtain h_o/d_o values below 0.1 for 2N2222 devices in TO-18 cans. Figure 3 shows the case where the wire is stretched

[4] G. Harmon, National Bureau of Standards; private communication.

to its maximum taughtness. In order to make the second bond at the post it is necessary for the wire to be looped in such a way as to avoid bumping the bonding tool against the side of the post. Consequently the wire bond operator is forced to form a loop in the wire. The worst case (i.e. smallest loop) shown in Figure 3 yields a figure of ~0.10 for h_o/d_o. In practice however the loop height is greater than that shown in Figure 3 because the operator allows a safety factor in order to avoid bumping the side of the post and h_o/d_o is significantly larger than 0.10. Figure 27 shows scanning electron micrographs of eight randomly chosen devices with Al-1% Mg wire bonds which were bonded for subsequent power cycling tests in a typical production operation. The loop heights are such that h_o/d_o is greater than 0.15 in all cases, even though there is a wide variation in loop heights. Consequently these bonds would all experience the same degree of flex from the previous mathematical calculation.

However, an additional factor must be considered in determining the effect of wire dress on fatigue life. When a small loop height is employed, the bonding tool has to be moved in a direct line towards the post. Since the initial bond is made by bringing the tool (with the wire running through the orifice in the tool (see Figure 28) at an angle of approximately 70^o to the die, any movement away from the die towards the post tends to flex the wire down and hence introduce a crack, or widen an existing crack in the heel of the bond. If a large loop height is used, the bonding tool initially moves in a direction more nearly normal to the die (parallel to the wire) before it is moved to the post. This prevents flexing of the wire and hence a minimization in the notch depth or size at the heel. Consequently, a bond with a large loop height is a more damage-free bond than one with a small loop height and is more reliable.

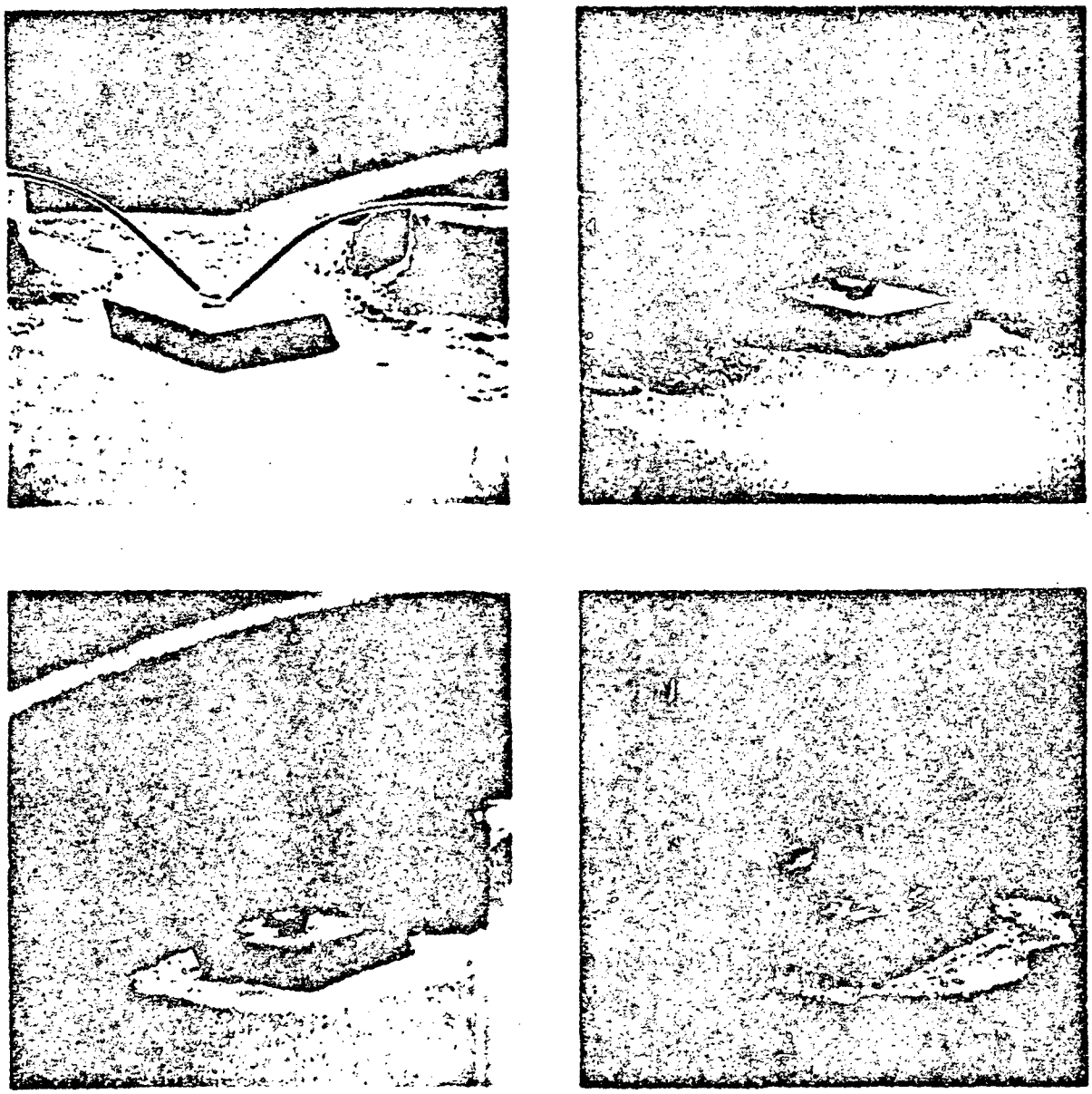

Figure 27. Scanning Electron Micrographs of Typical Devices Built Using Al-1% Mg Wire. Note the variation in the loop heights.

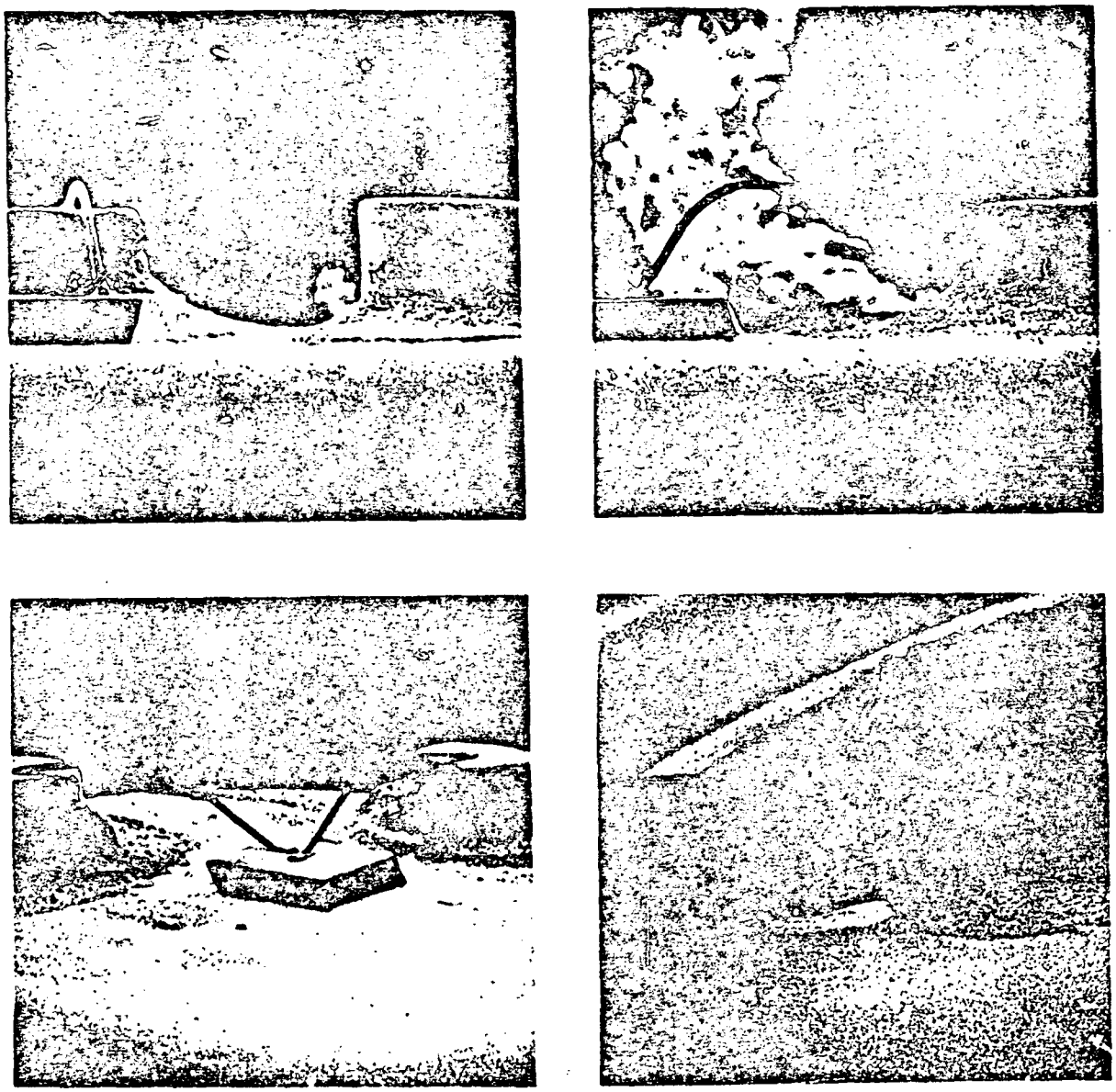

Figure 27. (Cont'd.)

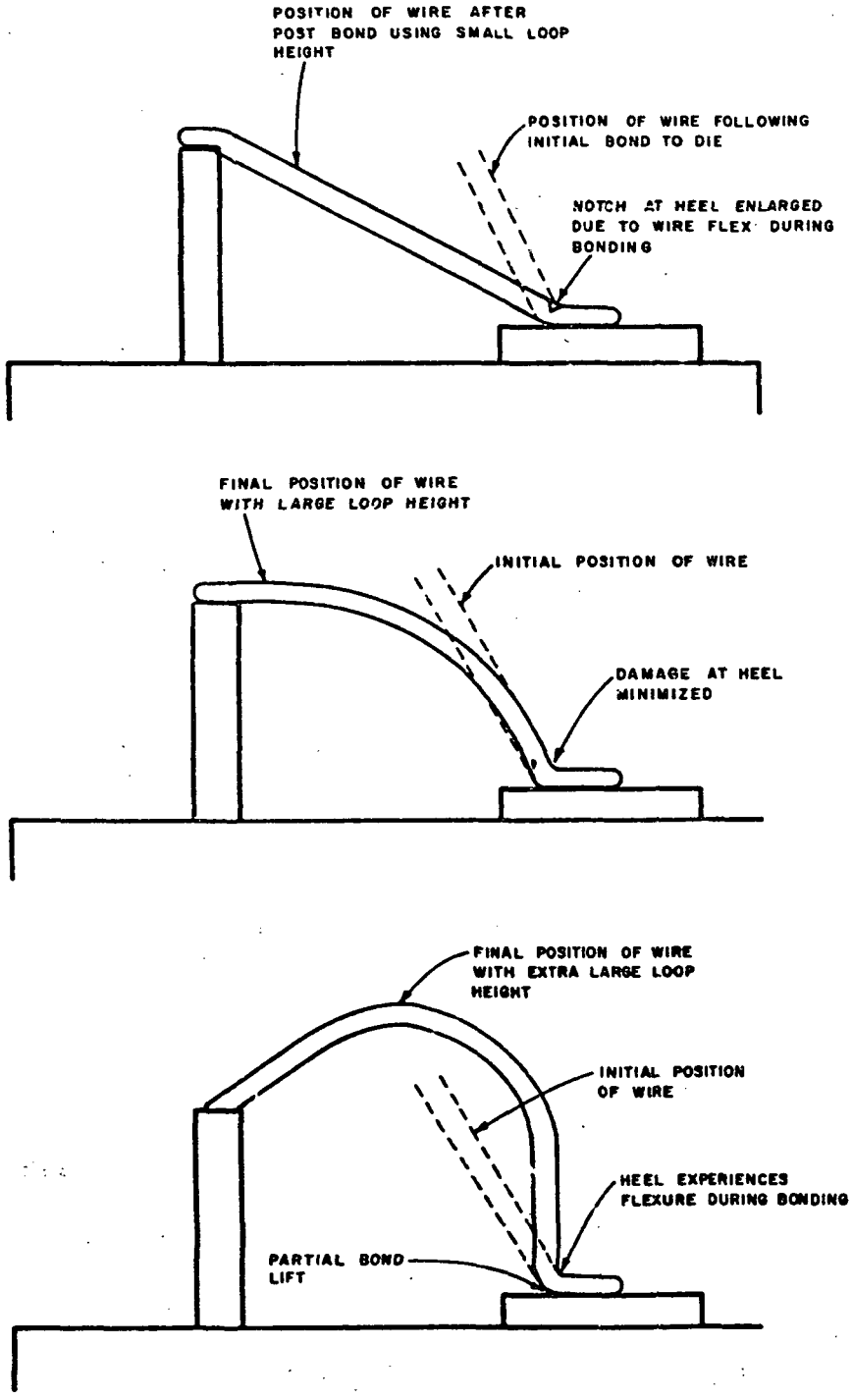

Figure 28. Effect of Wire Loop Height [illegible]age at the Heel of the Bond During Manufac[illegible]ure

A very large loop height with the wire normal to the die will also result in flexure of the wire during bonding as well as the possibility of lifting of the bond from the metallization. Figure 28 shows schematic sketches illustrating these points.

Figure 29 shows scanning electron micrographs of bonds made by two methods. In one case the first bond was made on the die and the second bond made on the post. This involved some flexure of the wire following the first bond with the result that a notch was created at the heel as shown in the top micrograph in Figure 29.

The bottom micrograph shows the bond on the die. In this case the bond was first made on the post and the second bond made on the die. In doing this no flexure was experienced by the bond on the die and hence as seen in the picture no crack is introduced in the heel of the bond. Of course the crack has now been transferred to the bond on the post and the failure mode will also be shifted to the post bond. However the significance of these experiments lies in the fact that the introduction or enlargement of a crack in the heel of the bond is a close function of degree of flexing experienced by the bond during bonding.

To summarize, it is undoubtedly true that the loop height may influence the degree of flex of the heel under certain conditions; i.e., when the wire is very taut. However, for 2N2222 devices on a TO-18 can it was shown that the minimum loop height to length obtainable in practice was greater than 0.1 and is generally greater than 0.15 because of the geometry of the system. It was shown that very taut loops and exaggerated loops create additional damage at the heel of the bond which shorten the fatigue life and should be avoided.

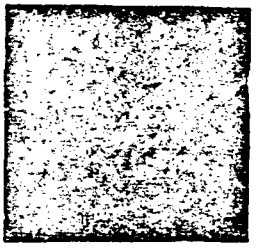

Bond on Die. Bonding Sequence --Die to Post. Crack Develop at Heel of Bond Due to Flexing During Bonding

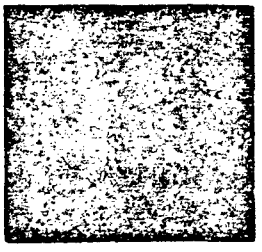

Bond on Die. Bonding Sequence -- Post to Die No Cracks at Heel. Cracks Transferred to Post Bond.

Figure 29.

SECTION IV

4.0 SUGGESTED PROCEDURES FOR IMPROVING THE RELIABILITY OF WIRE BONDS

Based on the results of this study, suggestions for improving the reliability of 1-mil aluminum wire bonds can be made.

(1) This study has shown that the most important variable is the material variable. The use of a solid solution hardened wire such as Al-1% Mg or a combination solid solution and stable dispersion hardened system such as Al-1% Mg - 0.5% Mn will significantly improve reliability.

Since the conventional Al-1% Si wire is susceptible to temperature induced coarsening its choice as a bonding material is not the best one. The use of wires with adequate strength and ductility which are retained after any elevated temperature treatments is recommended. Very high or low tensile strength wires tend to result in bonds with poor pull strengths and hence poor fatigue properties.

(2) Ultrasonic bonding should be used in preference to thermocompression bonding. Ultrasonic bonding causes less deformation and work hardening at the heel of the bond. From accelerated fatigue testing, it can be noted that ultrasonic bonding increases lifetime by a factor of two over thermocompression bonding. For comparison, switching to Al-1% Mg instead of Al-1% Si should increase lifetime more than a factor of five.

(3) Notches at the heel of the bond should be minimized to increase fatigue lifetime. (See Appendix I) This is accomplished by utilizing a moderate loop height in making the bond.

Also, by utilizing a solid solution hardened system such as Al-1% Mg, some degree of notching of the wire can be better tolerated than in the case of the dispersion hardened Al-1% Si system.

(4) The machine variables (pressure dwell time, ultrasonic power) for ultrasonic bonding should be optimized for each tensile strength of wire used.

2N2222 transistors have been fabricated using the above suggested procedures. The devices were bonded ultrasonically using Al-1% Mg wires 0.001 inch in diameter. Figure 30 shows the loop height used and the quality of the bond. Attempts were made to obtain a minimum of notching at the heel of the bond. These devices are being subjected to test procedures involving power cycling. The plan employed is as follows:

Power Cycling -

Pd = 500 mW

VCB = 10 V

IC = 50 mA

TA = 25°C

t (on) = 1 min, t (off) = 1 min (30 cycles per hour)

ss = 400 +*

* Two units withdrawn after every 500 hours and subjected to SEM analysis.

Four hundred and fifteen randomly selected devices were subjected to power cycling and readouts were obtained after 500 hours (15,000 cycles) and 1000 hours (30,000 cycles). At each of these points two devices were removed from the test for SEM

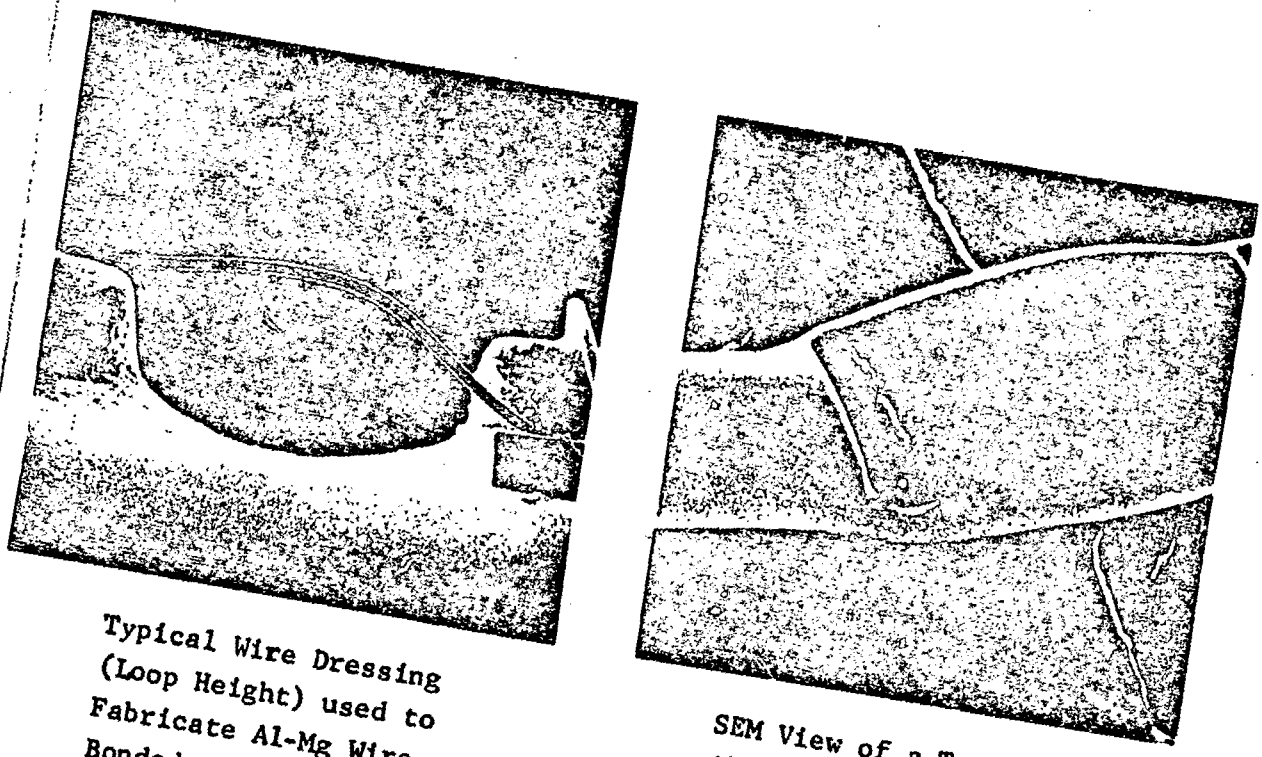

Typical Wire Dressing (Loop Height) used to Fabricate Al-Mg Wire Bonded Devices

SEM View of a Typical Al-Mg Ultrasonic Bond.

Figure 30. SEM Pictures Showing the Loop Height and the Quality of the Bond of Al-Mg Wire Bonded Devices.

analysis to determine the condition of the wire bonds. At present (30,000 cycles) no catastrophic failures have been obtained. Figure 31 show SEM photographs of the wire bonds after 15,000 cycles and 30,000 cycles respectively. No indication of the formation of microcracks was found in these (Al-Mg) wires. The remaining devices are now on test again and the power cycling will be continued beyond 50,000 cycles.

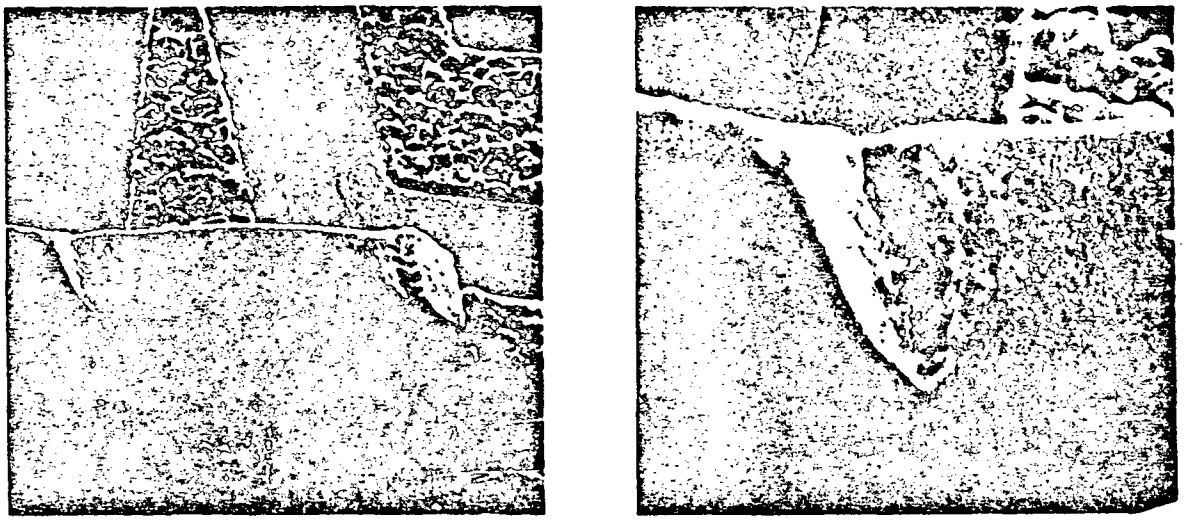

Quality of Bonds After 500 hrs. (15,000 cycles) of Power Cycling.
No Failures Noted at This Stage.

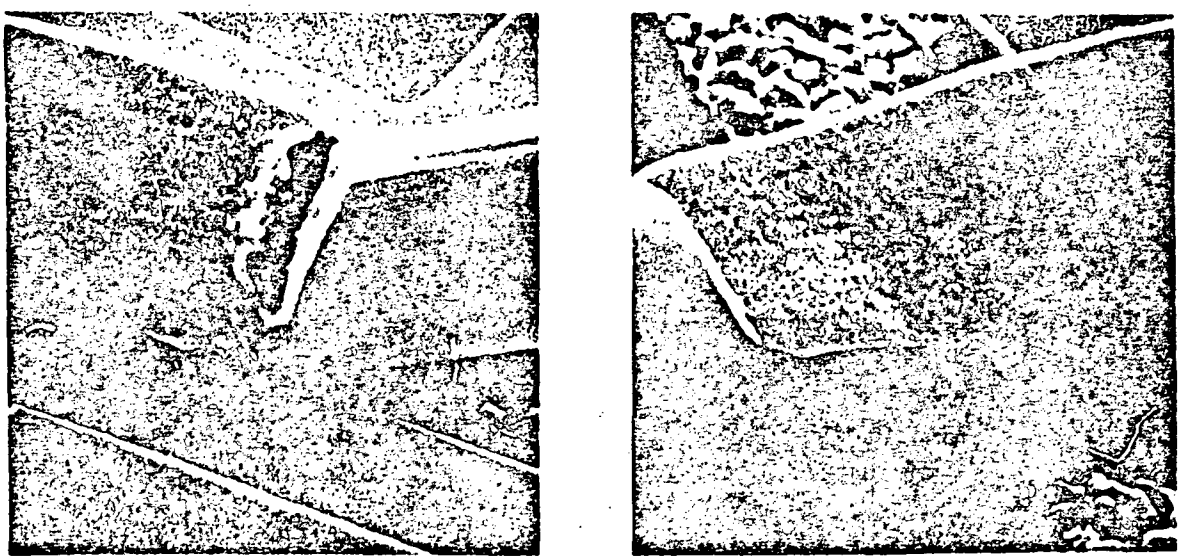

Quality of Bonds After 1000 hrs. (30,000 cycles) of Power Cycling.
No Failures Noted at this Stage. Note the Severe Surface
Reconstruction of the Al Metallization

Figure 31

9833-11-1

ACKNOWLEDGEMENTS

The author wishes to express his greatful appreciation to the following people for their help during the course of this work: J. Black, H. DaCosta, T. Gonzales, B. Heurta, D. Kirkman, L. Millikan, E. Philofsky, C. Thornton, S. Tasse, and C. J. Varker.

APPENDIX I

The nature of crack propogation in solids is a complicated phenomenon involving a number of variables such as the elastic moduli of the materials, the mode of application of the stress, the theoretical cohesive strength of the materials, the environment in which the materials are used, etc. However, probably the most important factor is the microstructure of the material. Propopation of cracks involves the expenditure of energy, the energy being that required to create new surfaces as the crack propogates in the solid. Among other factors this energy is a function of the sharpness of the tip of the moving crack or the radius of the crack tip. Sharper cracks can propogate more easily in the material and the way in which a moving crack can be stopped is to dissipate the energy of the crack by doing the work of plastic deformation rather than by cleaving atomic planes. This can be achieved in ductile materials which tend to plastically deform at the front of a moving crack and hence blunt the crack front or increase the radius of the crack tip. On the other hand, if a crack moves from a ductile phase into a brittle phase, the crack can no longer cause plastic deformation and hence expends its energy in cleaving the atomic planes. This means that the crack remains sharp or becomes sharper and keeps propogating. Consequently, in a system such as Al-Si, the presence of a crack or notch at the heel of the bond would be detrimental since this notch can be the source of microcracks during fatigue. These microcracks are not blunted by the metal since the dispensed brittle silicon particles allow rapid propogation of the cracks through them. The solid solution hardened system, Al-Mg, on the other hand, has no dispersed phases to affect the kinetics of crack propogation. A moving crack is more effectively stopped in this system because of the ductile nature of the medium in which the crack is propogating. Consequently, a notch of the kind shown

in Figure 6 can be better tolerated in the Al-Mg system. Figure (I-1) shows schematically the mechanism of crack propogation in the two systems, Al-Si and Al-Mg.

It is possible, however, to obtain a highly fatigue resistant dispersion hardened alloy if the dispersed phase is small in size and distrubuted uniformly and does not change with temperature. This, of cource, is not the case with Al-Si wires.

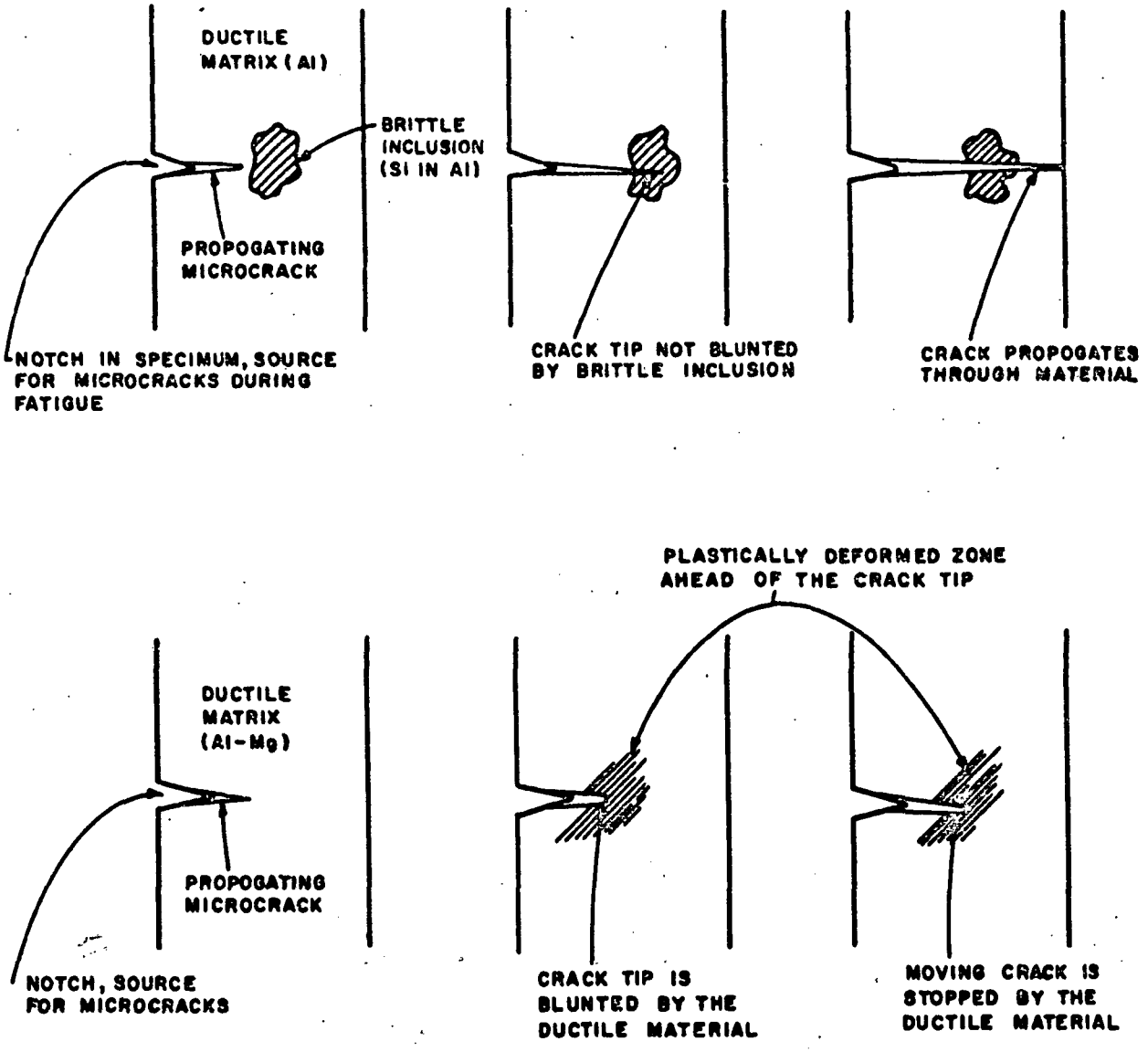

Figure I-1 Idealised Sketches of the Mechanism of Crack Propogation in Dispersion Hardened and Solid Solution Hardened Alloys.

9834-11-1

APPENDIX II

The Structure and Mechanical Properties of Fine Diameter Al – 1pct Si Wire

K. V. RAVI AND E. PHILOFSKY

The structure and mechanical properties of fine diameter Al–1pct Si alloy wires have been investigated. The mechanical behavior of wires as received from the vendor was found to vary greatly depending on the size and distribution of the silicon and on the strain rate of deformation. The ductility was found to increase with decreasing silicon particle size. In addition, wires with the finest silicon particle size (several hundred angstroms) were found to have a large increase in ductility over the strain rate range of 3 to 8 × 10⁻⁴ per sec. In this range these wires exhibited large yield drops followed by serrated yielding. Aging the wires at 200° to 450°C resulted in loss of strength and ductility.

BECAUSE of its compatibility with aluminum metallization and its drawability to diameters as fine as 0.7 mil, Al–1 pct Si wire is used extensively in the semiconductor industry for making interconnections between the semiconductor device and the package in which it is encased. These interconnections are achieved by plastically deforming the wire and metallization either by the application of temperature and pressure or ultrasonic energy and pressure. The wire bond can subsequently experience mechanical shock and cyclic stresses during processing and operation. Hence, the mechanical properties of this alloy wire will determine to a considerable degree the integrity of bond formation as well as the reliability of the bond.

Previous investigators have studied the structure[1,2] and mechanical properties[1,2,3,4] of low Si-Al alloys. Since the solubility of silicon in aluminum is negligible below 250°C,[5] the silicon in the wire would be present as a separate phase. Rosenbaum and Turnbull[1,2] have shown the number of silicon particles to be strongly dependent on the thermal history of the specimen, and Bohm[3] has shown that the yield strength and work hardening behavior will have a strong dependence on this number. In the case of fine wire, the heavy mechanical working-low temperature annealing cycle in addition to prior thermal history would be expected to affect the mechanical properties. Also, the fine geometry of the wire introduces unique problems in terms of obtaining uniformity of structure along the length of the wire. Consequently, the mechanical behavior of the wire can be expected to be different from the behavior of bulk alloys of the same composition and subjected to similar thermal treatments. The purpose of the present study is to determine the mechanical properties of the commercially available wire and to relate these to the microstructure.

EXPERIMENTAL PROCEDURE

All mechanical tests were conducted on a floor model Instron tensile tester using a strain rate of 8.3 × 10⁻⁴ per sec. Due to the fine diameter of the wires tested, the length-to-diameter ratio of the specimens was very large. A 1-in. gage length was employed in all the tests as this was the smallest length of wire that could be handled without difficulty.* Specimens were loaded in such a way as to avoid nonaxial loading. The large length-to-diameter ratio minimized any effects of nonaxial loading or grip effects. Due to the nonuniformity of the wire, multiple tests were conducted until reproducibility was obtained.

Structural investigation was made by using the electron microprobe, the scanning electron microscope and the transmission electron microscope. For electron microscopy the wires were electropolished in a perchloric acid solution and for the electron microprobe, the wires were mounted in plastic and polished flat.

*The manufacturers of fine wires used for interconnections generally use a 10" gage length and an Instron cross head speed of 1"/min. As will be shown later, these low strain rates (~2 × 10⁻³ sec⁻¹) do not permit a sensitive discrimination of the properties of different types of wires.

EXPERIMENTAL RESULTS

Mechanical Properties and Structure of As-Received Bonding Wire

The tensile properties of a variety of spools of 1 mil Al-1 pct Si bonding wire as obtained from various vendors were determined at a strain rate of 8.3 × 10⁻⁴ per sec. and using 1 in. gage length. The load-elongation curves of various wires are illustrated in Fig. 1. Each curve is representative of a number of curves obtained for the particular type of wire. It is seen that there is a wide variance in mechanical properties with strengths ranging from 6 to 20 g and percent elongation varying from 2 to 18.* In subsequent characterization and discussion, the wires will conveniently be divided into three types according to their ductility:

Type I – <3 pct elongation
Type II – 3 to 7 pct elongation
Type III – >7 pct elongation

It is observed that a striking feature of all Type III wires is the nonuniform nature of yielding. These

*The values for percent elongation for wires reported in this study were much greater in many cases than those reported by the manufacturers on the spool. This is due to the slower strain rate and smaller gage length used in this test.

K. V. RAVI and E. PHILOFSKY are Senior Metallurgist, and Manager, Metallurgy and Analytical Service Section, respectively, Central Research Laboratories, Motorola Semiconductor, Phoenix, Ariz.

This manuscript is based on a paper presented at the annual conference sponsored by the Electronic Materials Committee of the Institute of Metals Division of the Metallurgical Society of AIME and held August 30-September 2, 1970, in New York City.

wires display large yield drops followed by serrated yielding with increasing load. The causes of this behavior will be covered in the discussion.

In order to relate the mechanical behavior of the three types of wires to their fracture characteristics, a scanning electron microscope examination of the fracture surfaces was performed. The micrographs are illustrated in Figs. 2(*a*) through 2(*c*). Fig. 2(*a*) shows the fracture surface of a Type I wire to be that of a brittle fracture. The jagged edges indicate the

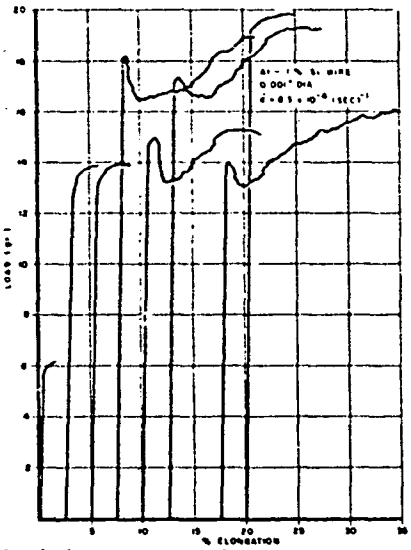

Fig. 1—Load-elongation curves for different Al-1 pct Si alloy wires. The curves have been offset along the strain axis for the sake of clarity.

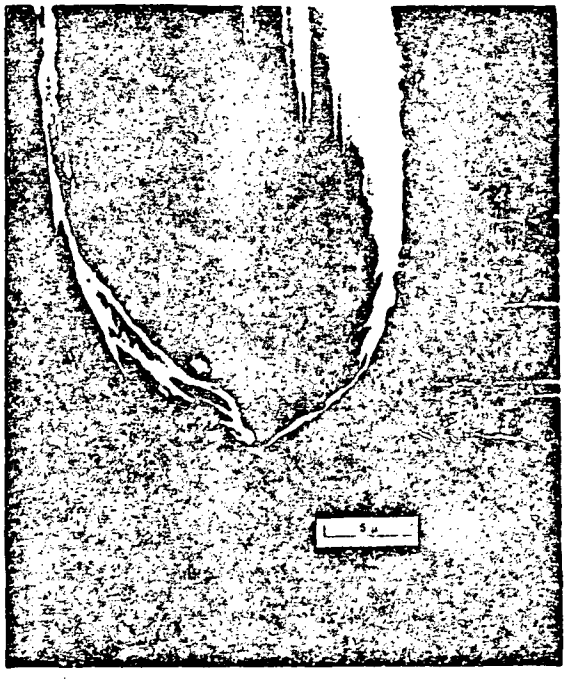

(*a*)

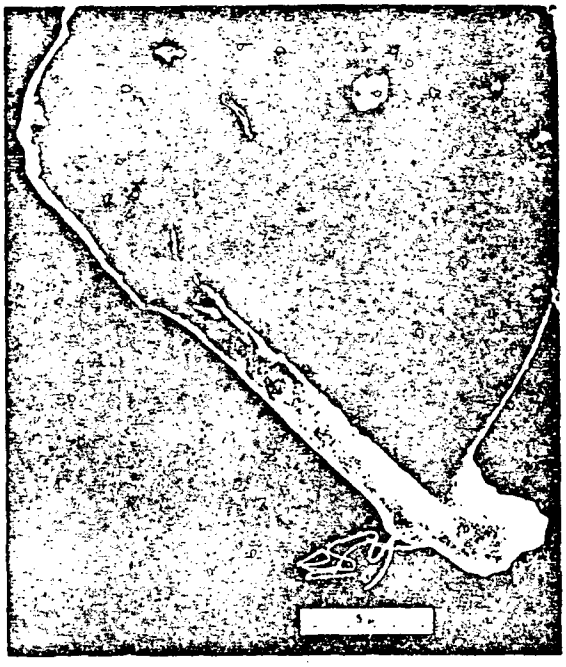

(*b*)

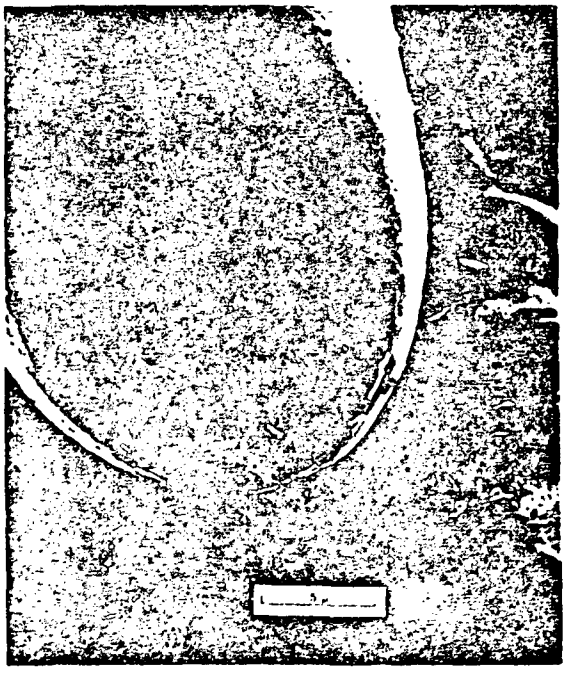

(*c*)

Fig. 2—Scanning electron micrographs of the fracture surfaces of the three types of wires: (*a*)—Type I; (*b*)—Type II; (*c*)—Type III.

wire failed through a local separation of the metal preceded by very little plastic flow. The Type II wire fracture surfaces exhibit evidence of some plastic flow although the mode of fracture is still brittle in nature, Fig. 2(*b*). The Type III wires have entirely ductile fracture characteristics, Fig. 2(*c*). The wires neck locally, and fail by means of a 'cup and cone' type of fracture.

The tensile properties and fracture characteristics of the wires can be related to the nature of the silicon dispersion in the aluminum matrix. Figs. 3(*a*) through 3(*c*) are silicon X-ray photographs of the three types of wires. It is observed in Fig. 3(*a*) that Type I wire has a nonuniform silicon dispersion with silicon particles as large as 2μ embedded in the aluminum. The Type II wires have a finer silicon dispersion with occasional large silicon particles, Fig. 3(*b*). Metallographic examination in the SEM (Scanning Electron Microscope) revealed an average silicon particle size of 0.2μ and a particle density of 10^{12} particles per cu cm. The Type III wires had a fine, uniform silicon dispersion as shown in Fig. 3(*c*) with individual silicon particles too small to be discerned by the microprobe or the SEM. Transmission microscopy revealed an average particle size of 200Å and particle density of 10^{15} per cu cm.

Strain Rate Effects

In order to determine the effect the rate of deformation has on strength and ductility of the wires, tests were conducted at different strain rates between 3.3×10^{-5} per sec. and 1.7×10^{-2} per sec. Fig. 4(*a*) shows load-elongation curves for a Type III wire at different strain rates. It is observed that the ductility of the wires has a maximum over a strain rate range of 3 to 8×10^{-4} per sec. Above and below this strain rate

(*a*)

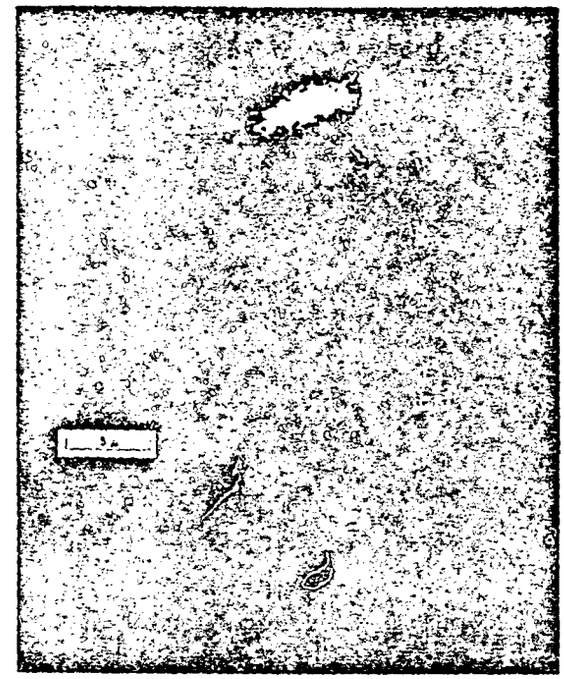

(*b*)

(*c*)

Fig. 3–Si-Kα X-ray photographs from the three types of wire: (*a*)–Type I; (*b*)–Type II; (*c*)–Type III.

range the ductility decreases to very low values. As would be expected for fcc metals, the yield and tensile strengths are not greatly affected by the change in the strain rate. The large ductility in the intermediate strain rate range is accompanied by serrated yielding of the wire. Fig. 4(*b*) is a plot of ductility as a function of strain rate for Types II and III wire. Type III wire displays a ductility maximum and serrated yielding over a strain rate range around 10^{-4} per sec., whereas no serrated yielding or ductility maximum was observed for Type II wire.

Elevated Temperature Aging Effects

Since thermocompression bonding and subsequent packaging operation subjects wires to elevated temperatures, a study was made of the effects of elevated temperature aging on the mechanical behavior. It is expected that aging will greatly affect the mechanical properties since coarsening of the silicon particles will result with the accompanying reduction in silicon particle density. For example, aging a Type III wire for 15 min at 250°C results in growth of silicon particles to 0.2 μ with a reduction of particle density to 10^{12} particles per cu cm.

Figure 5 is a plot of strength and percent elongation for a Type II and Type III wire after 15 min aging time at various temperatures between 200° to 450°C. The yield strength was taken to be the lower yield strength when a yield drop occurred and as the proportional limit when no yield drops were exhibited. It is observed that the wires lose strength with aging, and the initial strength differences between wires become very small after aging. The large ductility of the Type III wires disappears on aging, but it is still seen to be superior to the Type II over the temperature range investigated. It was observed, in fact, that aging of Type III wires above 200°C for longer than 30 sec resulted in loss of the ductility maximum and serrated yielding.

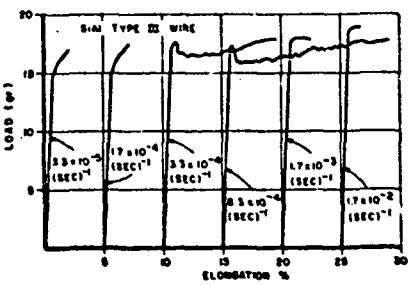

Fig. 4(*a*)—Load-elongation curves as a function of strain rate for a Type III wire.

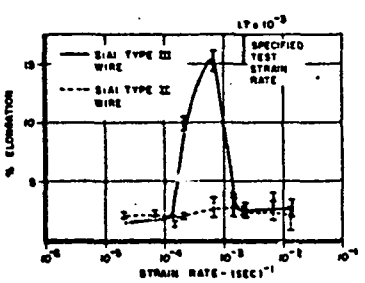

Fig. 4(*b*)—Percent elongation as a function of strain rate for Type II and Type III wires. The manufacturers' specified test rate is indicated. (Each data point represents an average of at least five tests.)

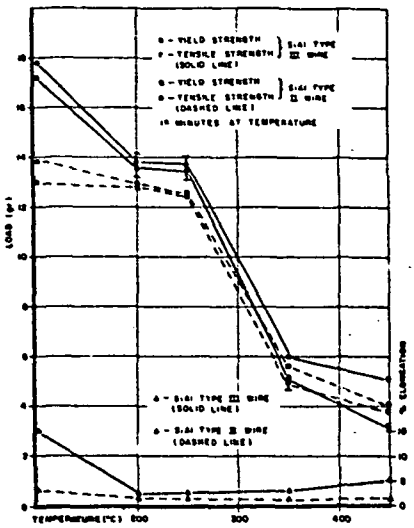

Fig. 5—A plot of the yield strength and the tensile strength as a function of aging temperature for two types of wires. At the bottom of the figure the percent elongation is plotted as a function of aging temperature. Strain rate = 8.3×10^{-4} $(sec)^{-1}$. (Each data point represents an average of at least five tests.)

The effect of aging on the fracture characteristics was also examined in the scanning electron microscope. Figs. 6(*a*) and 6(*b*) show fracture surfaces of Type II and Type III wire after aging at 450°C for 15 min. The very striking effect of heat treatment is seen in the development of sharp slip bands adjacent to the fracture surfaces in all wires aged at this temperature. The ductility differences in the two wires can still be observed in the less jagged appearance of the fracture surface of Type III wire.

DISCUSSION

Effects of Silicon Distribution

Both the strength and ductility of the wires were observed to be a function of the size and distribution of the silicon in aluminum. The most striking effect of silicon size and distribution was upon the ductility of the wires. When a uniform particle distribution with particle sizes of several hundred angstroms was present, a large ductility maximum at strain rates around 10^{-4} per sec was observed. This ductility maximum disappeared with increasing particle size, while the strength was maintained. A loss of strength is observed when the silicon particle size increases above 2 μ.

Since the ductility maximum is accomplished by serrated yielding the origin of the ductility is related to dislocation-dispersed phase interaction. A fine dispersion of silicon causes dislocation locking and unlocking thereby extending the region of the wire under-

going deformation. This situation is analogous to the propagation of a Luders band in a single crystal.[6] The deformation is not confined to a few slip plans but a number of slip sources become activated because of the impeding of dislocations by the dispersed silicon. Growth of the particles by aging the wires results in a loss in strength and ductility. Slip becomes confined to those regions of the wire which are relatively free of silicon due to agglomeration and growth of silicon in other regions of the wire. This behavior is reflected in the development of deep, coarse slip bands following deformation of aged wires, Figs. 6(*a*) and (*b*). Slip bands are not observed in the unaged wires, Figs. 2(*a*) through (*c*).

Aging would also have the effect of annealing the wires which at higher temperatures could result in grain growth. The grain growth will be preferential due to the internal strain that exists in the unannealed wires. At longer aging times it is possible to develop a 'bamboo' structure consisting of single crystalline regions along the wire. Fig. 7 shows such a structure developed in a wire aged at high temperatures. This is analogous to the strain anneal technique for growing single crystals. The development of a large grain size with preferred orientation could also account for the sharp slip bands observed in the aged wires, Figs. 6(*a*) and (*b*).

Serrated Yielding

Serrated yielding in the wires is always observed to begin at zero plastic strain, Fig. 1. In previous studies of serrated yielding in fcc substitutional alloys, the onset of serrations has always been observed only after a certain degree of prestrain.[7,8] This is an important

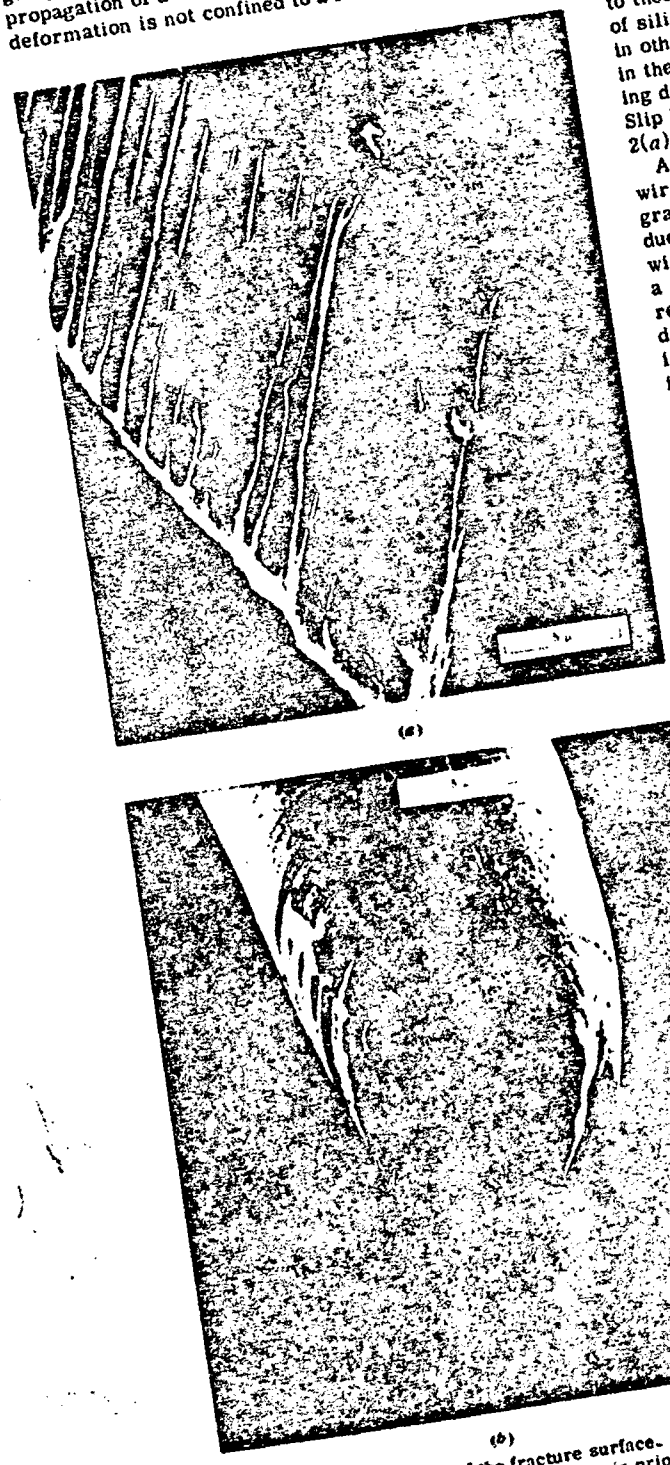

(*a*)

(*b*)

Fig. 6–SEM photographs of the fracture surfaces of Types II and III wires after aging at 450°C for 15 min prior to testing: (*a*)–Type II; (*b*)–Type III.

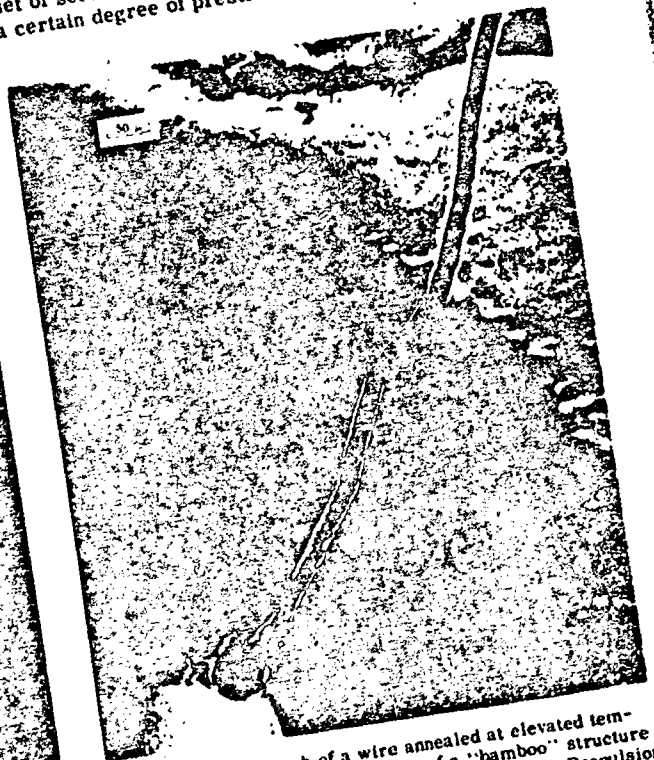

Fig. 7–SEM photograph of a wire annealed at elevated temperatures showing the development of a "bamboo" structure (SEM photograph courtesy of J. Devaney of the Jet Propulsion Laboratory, Pasadena, Calif.)

difference of the present results from the classical concept of the Portevin-Le Chatelier effect.[9] The onset of serrations at zero plastic strain has been reported in some interstitial alloys of the fcc metals.[10] In this case the diffusion rate of interstitial atoms at room temperature is sufficiently high to cause dynamic strain aging effects and hence produce serrated yielding. In substitutional alloys the solute diffuses much too slowly at room temperature to produce dynamic strain aging. However, after prestrain, serrated yielding is observed in these materials. This is explained on the basis that cold work creates vacancies which enhance the diffusivity of the solute atoms and produces the phenomena of repeated yielding.

The onset of serration in the fine diameter Al-Si wires is, in all cases, preceded by large yield drops as shown in Fig. 1. In the absence of a yield drop, no serrated yielding was observed and the ductility was correspondingly low. The disappearance of yield drops and serrated yielding occurred when the silicon particle size increased as well as when the strain rate of deformation exceeded 8.3×10^{-4} per sec and decreased below 3.3×10^{-4} per sec.

The strain rate of deformation $\dot{\epsilon}$ can be related to the mobile dislocation density ρ and the diffusivity of the solute species D as follows[11]

$$\dot{\epsilon} \simeq \rho D$$

Since the diffusivity of silicon in aluminum is far too low to cause serrated yielding at room temperature, the rate controlling process for the onset of serrated yielding is the pinning of fast moving dislocation which were earlier generated by the yield drop phenomena.[12] A large increase in the mobile dislocation density that takes place when a yield drop occurs causes unstable plastic flow by dislocation pinning and depinning with further increase in strain.

It has been found[7,13] that serrated yielding in single crystals occurs after much larger strains than in polycrystals at the same temperature and strain rate. This is based on the fact that single crystals would have a lower initial mobile dislocation density than polycrystals. For a critical mobile dislocation density to be reached to cause serrated yielding larger prestrains are required for single crystals than for polycrystals. Hence, for serrated yielding to occur in fcc substitutional alloys, a large mobile dislocation density or a large strain-induced vacancy concentration is necessary. In the case of Al-Si wires, the initial yield drops produces a large mobile dislocation density to initiate serrated yielding.

Discontinuous yielding is strain rate dependent as well as being a function of the size and distribution of silicon. Hirth[14] has discussed the effect of temperature on the onset and ending of serrated yielding. An analogous explanation can be given for the effect of strain rate. At low strain rates the velocity V_c of dislocation is too low to break away from pinning points or to multiply rapidly by cross slip. Consequently, the deformation process cannot be described by the strain-rate equation for plastic flow:

$$\dot{\epsilon} = \rho b V$$

where $\dot{\epsilon}$ is the strain rate of deformation, ρ is the mobile dislocation density, b, is the Burgers vector and V is the dislocation velocity. At the critical strain rate the slow moving dislocation will break away from pinning points to form fast dislocations with a velocity V_p which controls deformation. At this critical imposed strain rate the fast moving dislocations will be repinned by the silicon particles to result in serrated yielding. At higher strain rates the velocity of the dislocations will be sufficiently high as to satisfy the strain rate equation and serrated yielding will no longer be observed. The motion of the crosshead is fast enough to accommodate the rapid decrease in the stress due to dislocation multiplication thus obliterating the microscopic yield drop. In general, it is also observed, Fig. 1, that serrated yielding is accompanied by higher work hardening rates as would be expected for materials with a large dislocation density.

The Nature of the Yield Drop

Due to the inherent problems of manufacturing wires of diameters of 0.001 in. or less, uniformity of structure cannot be easily maintained. The Al-Si wires have been observed to be quite nonuniform in terms of their structure and mechanical behavior. One unusual manifestation of the nonuniformity is a variation in the nature of the yield drop exhibited by specimens of a wire taken from different regions of a long sample. Fig. 8 shows representative examples of the yield drops observed for the same wire. The yield drop varied from a well-rounded gradual drop to a sharp and sudden drop. This behavior is explained on the basis that a nonuniformity of structure can exist both in terms of an agglomeration of silicon as well as a variation in the dislocation density at different regions of the same specimen.[15] This has been confirmed by microprobe analysis and electron microscopy. If a low mobile dislocation density exists the yield drop would be rounded

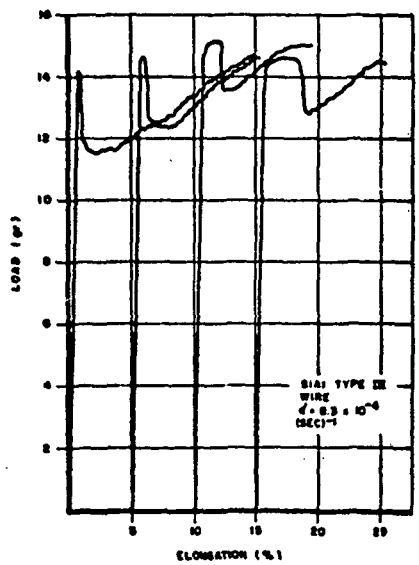

Fig. 8—Load-elongation curves of different specimens of a Type III wire showing the variety of yield drops exhibited by this material.

Fig. 9—Transmission electron micrograph of a Type III wire showing dislocation pinning by the dispersed silicon.

and gradual, reflecting a Gilman-Johnson[16] type of dislocation multiplication phenomena involving a double cross slip mechanism. If, on the other hand, the dislocations are initially pinned by silicon particles, yielding will take place by a Cottrell[17] type breakway phenomenon resulting in a sharp and sudden yield drop. In either case, an increase in the mobile dislocation density results with the accompanying initiation of serrated yielding. Some evidence for dislocation pinning by dispersed silicon particles was obtained by transmission electron microscopy as shown in Fig. 9.

CONCLUSIONS

A wide variation in the mechanical behavior of Al-1 pct Si wires has been observed. These properties are found to be a function of the silicon dispersion, the size of the dispersed phase and the strain rate of deformation.

For wire bonding applications a low strength and ductility will result in the formation of weak bonds due to the excessive bond deformations during the bonding process, as well as in poor fatigue properties of the bond so formed. Reliability of such bonds will be questionable. Large ductility values will permit acceptable bond deformation while at the same time forming a good bond which will not be susceptible to fatigue-induced failure during service.

ACKNOWLEDGMENTS

We wish to thank Mr. A. Gonzales and Mrs. L. Millican for their excellent analytical work on the electron microprobe and scanning electron microscope. We also thank Mr. D. McKinstry and Mrs. V. Rysso for their experimental assistance.

REFERENCES

1. H. S. Rosenbaum and D. Turnbull: *Acta Met.*, 1958, vol. 6, p. 653.
2. H. S. Rosenbaum and D. Turnbull: *Acta Met.*, 1959, vol. 7, p. 664.
3. H. Bohm: *Acta Met.*, 1963, vol. 11, p. 475.
4. Zoku Bakkoishi: *Nippon Kin.*, 1965, vol. 29, (4), pp. 406-11.
5. *Constitution of Binary Alloys*, M. Hansen, ed., pp. 132-34, McGraw-Hill Book Co., 1958.
6. J. Weertman and J. R. Weertman: *Physical Metallurgy*, R. W. Cohn, ed., p. 769, North-Holland Publishing Co., Amsterdam, 1965.
7. B. J. Brindley and P. J. Worthington: *Acta Met.*, 1969, vol. 17, p. 1357.
8. P. G. McCormick: *Scripta Met.*, 1970, vol. 4, p. 221.
9. A. Portevin and F. Le Chatelier: *Acad. Sci., Compt. Rendus*, 1923, vol. 175, p. 507.
10. J. S. Blakemore: *Met. Trans.*, 1970, vol. 1, pp. 165, 151.
11. T. Bonisewski and G. C. Smith: *Acta Met.*, 1963, vol. 11, p. 165.
12. A. S. Keh, Y. Nakada, and W. C. Leslie: *Dislocation Dynamics*, p. 381, McGraw-Hill Book Co., New York, 1968.
13. W. Chr[illegible]: *Phil. Mag.*, 1968, vol. 18, p. 89.
14. J. P. Hirth: *Dislocation Dynamics*, p. 407, McGraw-Hill Book Co., New York, 1968.
15. J. D. Campbell, R. H. Cooper, and T. J. Fischhof: *Dislocation Dynamics*, p. 723, McGraw-Hill Book Co., New York, 1968.
16. W. G. Johnston and J. J. Gilman: *J. Appl. Phys.*, 1959, vol. 30, p. 129.
17. A. H. Cottrell: *Dislocation and Plastic Flow in Crystals*, Clarendon Press, Oxford, 1953.

Appendix III

Sections of Phase Diagrams of Different Al Alloys Investigated for Bonding Applications

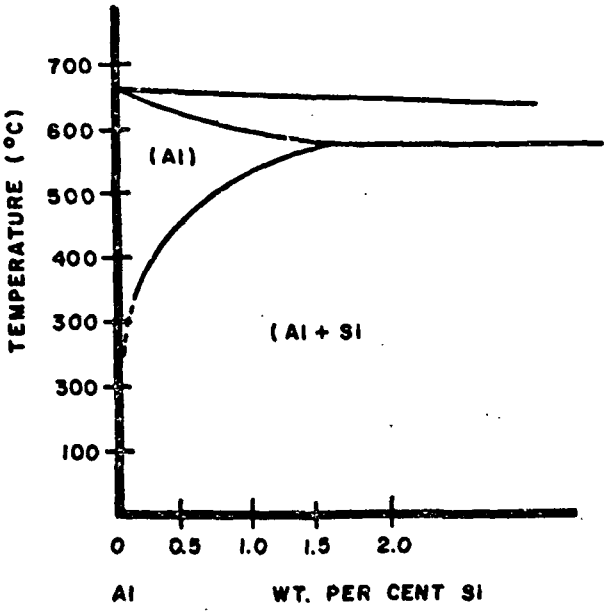

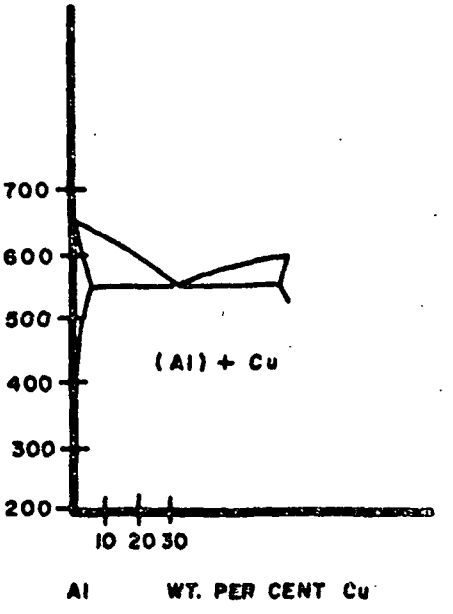

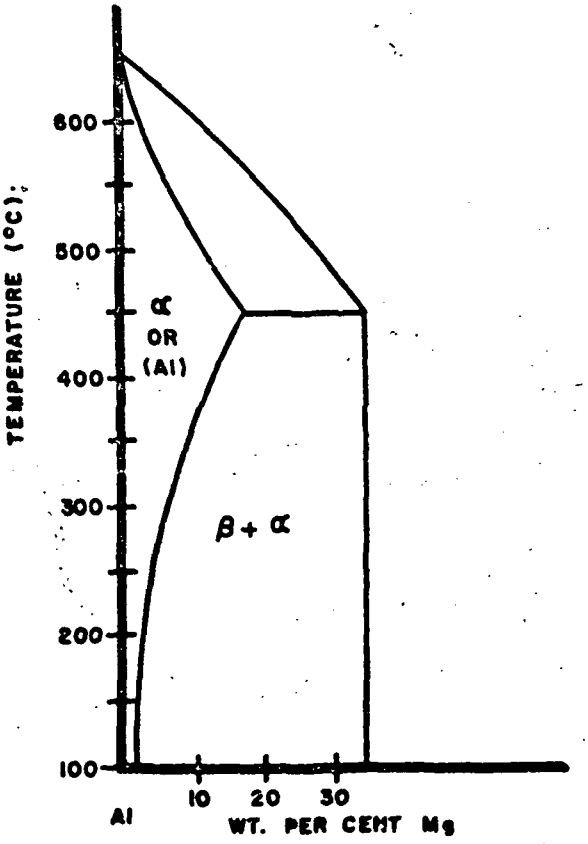

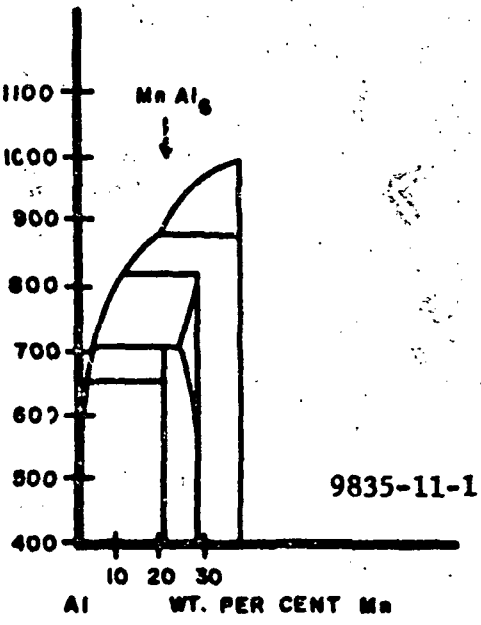

9835-11-1